Source Generated Electrostatic Waves in a Plasma-
With Application to the Earth's Electron Foreshock Region

by

Michael Joseph Pangia

A dissertation submitted in partial fulfillment
of the requirements for the degree of

Doctor of Philosophy

University of Washington

1988

Approved by George C. Parks
(Chairperson of Supervisory Committee)

Program Authorized
to Offer Degree Physics

Date 12-15-87

Doctoral Dissertation

In presenting this thesis in partial fulfillment of the requirements for the Doctoral degree at the University of Washington, I agree that the Library shall make its copies freely available for inspection. I further agree that extensive copying of this dissertation is allowable only for scholarly purposes, consistent with "fair use" as prescribed in the U.S. Copyright Law. Requests for copying or reproduction of this dissertation may be referred to University Microfilms, 300 North Zeeb Road, Ann Arbor, Michigan 48106, to whom the author has granted "the right to reproduce and sell (a) copies of the manuscript in microform and/or (b) printed copies of the manuscript made from microform."

Signature Michael J Pazzani

Date December 21, 1987

UNIVERSITY OF WASHINGTON

Abstract

SOURCE GENERATED ELECTROSTATIC WAVES IN A PLASMA- WITH APPLICATION TO THE EARTH'S ELECTRON FORESHOCK REGION

by Michael Joseph Pangia

Chairperson of the Supervisory Committee: Professor George K. Parks
Department of Physics

The problem of electrostatic waves generated in a collisionless plasma by a source of charged particles is formulated using the Vlasov description with an inhomogeneous term. A formal solution is obtained by use of the Green's function for the linearized case of a Maxwellian background plasma with a low density particle source. Detailed analysis of the Green's function shows the dynamic behavior of the system as time progresses. In particular, in addition to the asymptotic time limit of the Green's function being described by the roots of the dielectric function, two other limits are discussed. The short time limit of the Green's function behaves approximately like a cold plasma, and the intermediate time limit of the Green's function behaves approximately like a plasma with thermal electrons and a cold ion distribution.

An equation for the discrete Fourier transform coefficients of the electric field is derived without restricting to any particular time limit, and is useful for comparing with measured spectra. The theory is applied to the region deep in the Earth's electron foreshock where electrostatic waves are observed, and yet no beams to cause an instability have been reported. It is postulated that the electrostatic waves in this region are driven by the distribution of electrons coming from the bow shock, and that this distribution varies spatially with a characteristic wavelength. The electric field spectrum is calculated and shown to give agreement with the reported observations.

TABLE OF CONTENTS

LIST OF FIGURES

ACKNOWLEDGEMENTS

In completing this dissertation, I recall my heartfelt appreciation for the quality education I have received throughout my school years. I express my gratitude to the Stamford, Connecticut public school system for instilling and nourishing the desire to learn math and science, to the Cooper Union School of Engineering for pushing my abilities to great limits, to the Michigan State University Physics Department for giving me a solid foundation in graduate physics, and to the University of Washington Physics Department for their promoting good research skills by encouraging a student to learn on one's own.

I am grateful for the careful reading of my dissertation by Professors K. C. Clark and V. Ozols. I especially thank my advisor G. K. Parks for his valuable comments and continued support throughout my graduate studies at the University of Washington. I also thank the other members of the Space Science Program; in particular, R. H. Holzworth for his contributions to my understanding of Space Plasma Research, and D. W. Potter for the use of his typesetting program.

I am indebted to my parents, brothers and sisters, and grandmother for their enthusiastic support and personal sacrifices which enabled me to devote my time and energy to my studies. My wife Laura is also deserving of my gratitude for her assistance in word processing, and for her patience, love and understanding, which helped ease the stress associated with getting a Ph.D.

This work was supported in part by the National Aeronautics Space Administration, grant NAG5-373, and the National Science Foundation, grant ATM-8300164.

ONE

Introduction

The linear kinetic theory of electrostatic oscillations in a collisionless, unmagnetized plasma has been solved by Landau using the Vlasov equation along with Gauss' law [*Landau,* 1946]. These equations are homogeneous, and can be solved for the first-order particle distribution functions and the resulting electric field once having specified the particle distributions at some time. For later reference, the problem of solving this pair of homogeneous equations will be referred to as the *Landau problem.* It is the purpose of this thesis to consider the more general case of an inhomogeneous version of the linearized Vlasov equation. The inhomogeneous term can, for instance, be due to an injection of charged particles into the plasma. Appropriately, the problem of solving the homogeneous Vlasov equation coupled with Gauss' law is identified as the *plasma source problem* or simply the *source problem.* The source problem will be restricted to cases where both the inhomogeneous term (or, equivalently, the source term) and the first-order particle distributions vanish in the infinite past.

The source term can represent many naturally occurring or experimentally produced (such as an injection experiment) situations. In practice, one may define an

external supply of charged particles as a population of charged particles originating from a region of space other than the space occupied by the plasma under observation. A case where the external supply is clearly identifiable is that of an active experiment involving either the injection of particles into a plasma environment, or the generation of an electric field by means of a transmitting antenna. Examples are the Araks project which involved the injection of an electron beam into the magnetosphere from a rocket [*Cambou et al.,* 1980], and the SEPAC (Space Experiments with Particle Accelerators) experiment flown on the Spacelab 1 shuttle mission [*Neubert et al.,* 1986]. For these experiments the source region (region over which the source term can be non-zero) would be defined by the space occupied by the respective spacecraft. As another example, the sounder experiment aboard the satellite ISEE 1 generates an electric field by a transmitting antenna which later receives the refracted signal [*Harvey et al.,* 1978]. In this case, the antenna current during the transmitting mode would be provided by the power supply aboard the spacecraft. One would consider the power supply as the source of charged particles which make up the current. And here again, the source region is confined to the spacecraft boundary itself. Parenthetically, spacecraft charging, which occurs for injection experiments, would also contribute to the source term.

A source term can also be used to represent physics that otherwise may be complex for modeling. One such example exists when a portion of a flowing plasma is diverted toward another region of the plasma. The diversion might be a result of the plasma encountering a boundary which reflects a portion of the plasma back into the oncoming flow. The region of the plasma into which the reflected particles enter would then be subject to an external source of electric field (external in the sense that

the reflected particles supply this region of plasma with an additional charge density). One can study the effect the reflecting boundary has on the main flow by using an appropriately chosen source term. In particular, this use of the source problem would be applicable to the upstream region of the earth's bow shock. The bow shock behaves like a source of charged particles (with respect to the upstream region) supplying a population of reflected particles to the solar wind flowing toward the bow shock [*Klimas,* 1985].

In applying the source problem, a greater variety of electric field behavior may occur than for the Landau problem for several reasons. One reason is that an electric field may be initiated with every injected parcel of charged particles. This means the particles coming from the source bring into the plasma an electric field which was not previously there. Consequently, the plasma experiences local accelerations resulting in an induced electric field. As established by the Landau problem for Maxwellian plasmas, this induced or plasma generated electric field will damp away. But the overall process is capable of recurring with the introduction of each parcel of injected particles. The source would then be replenishing the electric field in competition with the damping process.

Owing to the damping of the electric field in the plasma medium, a major contribution to the total field at a given time is likely to be the portion of the electric field which was most recently initiated by the source. In an effort to accurately describe the recently produced portion of the electric field, this thesis will use the results of the equations in their entirety. This approach is to be contrasted with the solution of the Landau problem which, in practice, deals only with the asymptotic

time behavior [*Landau,* 1946]. In the asymptotic time limit, the electric field has frequencies (with corresponding damping rates) given by the roots of the dielectric function. Furthermore, the asymptotic limit describes the solution by the least damped of these roots. (For an unmagnetized plasma, the possible least damped frequencies correspond to the Langmuir and ion-acoustic modes.) But using an asymptotic description for the source problem will poorly approximate a significant portion of the electric field, and therefore this approach will not be used.

The more general approach will, enroute to solving the source problem, actually enhance one's understanding of the Landau problem. In fact, frequent comparison will be made to the Landau problem, as it is closely related to the source problem. That they are related is clear from the statement of the respective problems. The Landau problem, on the one hand, finds the electric field in a source-free plasma based on specifying the particle distribution at a given time (the initial condition). On the other hand, the source problem determines the electric field from knowing the source term. The source term, as noted earlier, introduces an electric field to the plasma medium and the plasma responds. In this respect, the source term and the initial condition are similar because the initial condition determines the electric field that the source-free plasma responds to.

To make the similarities more transparent, consider the form of the solutions, starting with the Landau problem. The electric field for the Landau problem, E_L, is commonly expressed by an inverse Laplace transform [*Nicholson,* 1983] (considering the one-dimensional case with no external fields)

$$E_L(t,k) = 4\pi \int_{-\infty+i\sigma}^{\infty+i\sigma} \frac{dz}{2\pi} \frac{\rho_L(z,k)}{ik\varepsilon(z,k)} e^{-izt} \qquad (1\text{-}1)$$

where

$$\rho_L(z,k) = -i\sum_a q_a \int dv \, \frac{f'_a(t=0,k,v)}{z-kv} \quad .$$

The real parameter σ appearing in (1-1) is chosen to be larger than the imaginary part of all poles in the integrand. $f'_a(t,k,v)$ is the spatial Fourier transform of the first-order distribution function of wave number k and velocity v for species a. Its normalization will be defined in Chapter 2. Here, the time variable t is restricted to non-negative values with $t=0$ being the time at which the initial condition is specified. ε is the dielectric function, and is independent of the initial condition $f'_a(0,k,v)$.

By applying the convolution theorem for Laplace transforms, (1-1) is cast in the desired form for interpretation.

$$E_L(t,k) = \frac{4\pi}{ik} \int_0^t dt_1 \, \varepsilon^{-1}(t-t_1,k) \, \rho_L(t_1,k) \qquad (1\text{-}2)$$

where $\varepsilon^{-1}(t,k)$ stands for the inverse Laplace transform of $1/\varepsilon(z,k)$. Computing $\rho_L(t,k)$ one finds

$$\rho_L(t,k) = \sum_a q_a \int dv \, f'_a(t=0,k,v) e^{-ikvt} \quad . \qquad (1\text{-}3)$$

The meaning of ρ_L can be easily identified by noting that $f'_a(0,k,v)e^{-ikvt}$ is the portion of the particle distribution that developed from the initial condition $f'_a(0,k,v)$. The distribution which appears as the integrand in (1-3) is known as a *free-streaming* distribution [*Krall and Trivelpiece,* 1973] because it evolves like a system which does not experience any forces; namely,

$$(\partial_t + ikv) f'_a(0,k,v) e^{-ikvt} = 0 \qquad (1\text{-}4)$$

with ∂_t denoting $\partial/\partial t$. Then from (1-3), one clearly recognizes $\rho_L(t,k)$ as the charge

density of the free-streaming distributions.

(1-2) illustrates the point made earlier that the initial condition is analogous to the source term. The electric field of the charge density ρ_L elicits a response from the plasma, as does the applied electric field in the source problem. E_L is the sum of two electric fields: one is the field of the charge density ρ_L (the applied field), and the other corresponds to the plasma response (the induced field). This implies $\varepsilon^{-1}(t,k)$ can be expressed as a sum of a delta function in time plus a term describing the induced electric field. The form of (1-2) is that of an integral of the product of the kernel $\varepsilon^{-1}(t-t_1,k)$ and the driving term $\rho_L(t_1,k)$, showing E_L satisfies an inhomogeneous equation as does the electric field for the source problem [*Morse and Feshbach,* 1953]. As a kernel, $\varepsilon^{-1}(t-t_1,k)$ determines the contribution of the charge density ρ_L at time t_1 to the electric field at time t. There is, strictly speaking, a contribution to the electric field at time t due to $\rho(t_1,k)$ for $0<t_1<t$, and the corresponding time range for the kernel $\varepsilon^{-1}(t-t_1,k)$ behavior is $t>t-t_1>0$. Therefore, using the asymptotic time expression for $\varepsilon^{-1}(t-t_1,k)$ for a given time t may be a poor approximation if $\rho_L(t)$ is not negligible.

The electric field for the source problem, $E(t,k)$ (with t taking on any value), can be expressed in a fashion similar to (1-2) as will be shown in Chapter 2, or based on a general knowledge of inhomogeneous linear equations [*Morse and Feshbach,* 1953]

$$E(t,k) = \int_{-\infty}^{\infty} dt_1\, G(t-t_1,k)\rho(t_1,k) \qquad (1\text{-}5)$$

$$= \int_{-\infty}^{t} dt_1\, G(t-t_1,k)\rho(t_1,k) \quad .$$

The latter equality follows from the fact that $G(t-t_1,k)$ is a Green's function, which vanishes for $t<t_1$. $G(t-t_1,k)$ obeys an equation similar to the equation satisfied by the electric field except that $\rho(t,k)$ is replaced by a delta function in time. Analogous to

ρ_L, $\rho(t,k)$ is the charge density of the particles coming from the source.

The only difference in form between (1-2) and (1-5) is the lower integration limit because the initial condition for the source problem is specified in the infinite past. Therefore, the discussion in a previous paragraph concerning the limitations on using the asymptotic expression for $\varepsilon^{-1}(t-t_1,k)$ applies to the kernel $G(t-t_1,k)$. That is, for time periods when the source charge density exists (or, is not negligible), the asymptotic limit for $G(t-t_1,k)$ may be a poor approximation.

An important similarity between (1-2) and (1-5) is established by considering a particular choice for ρ. Specifically, consider a source term (the inhomogeneous term added to the Vlasov equation) such that as $t\to 0^+$ the plasma has the same particle configuration as a Landau problem at that time, and then for $t>0$ the source term is zero. Here, $t\to 0^+$ indicates taking the limit of t going to zero while keeping t positive, thereby allowing for a discontinuity. The electric field for the Landau problem and the source problem would be the same for $t>0$ because then the two problems obey identical equations with identical initial conditions in the limit $t\to 0^+$. As a further consideration, use the following source charge density ρ

$$\rho(t,k) = \theta(t)\rho_L(t,k) \tag{1-6}$$

with $\theta(t)$ being the step function (1 if $t>0$, 0 if $t<0$). For such a choice, (1-5) becomes

$$E(t,k) = \theta(t)\int_0^t dt_1\, G(t-t_1,k)\rho_L(t_1,k) \quad . \tag{1-7}$$

Since this is equal to the solution of the Landau problem (1-2), one sees that $ikG(t,k)$ and $4\pi\varepsilon^{-1}(t,k)$ must contain common information for $t>0$.

The stronger statement that

$$ikG(t,k) = 4\pi\varepsilon^{-1}(t,k) \quad ,t>0 \tag{1-8}$$

is arrived at by noting this analysis must hold for all possible $\rho_L(t,k)$. As anticipated, the physics of the two problems have much in common. They differ in the time at which an electric field is introduced into the system. For the source problem, with each parcel of injected plasma there is an associated electric field brought into the system. For the Landau Problem, after t=0 the system simply evolves without any externally supplied electric field.

Thus far, the importance of the source problem, relative to the Landau problem, has been established. One would also like to compare features of the source problem to reported observations. A quantity often measured is the frequency power spectrum of the electric field, which can be compared to the transform of (1-5). The time dependence of (1-5) is easily Fourier transformed by applying the convolution theorem to the first of the two equations, resulting in the relation

$$E(\omega,k) = G(\omega,k)\rho(\omega,k) \tag{1-9}$$

with ω as the Fourier transform variable, which is real. This equation shows the spectrum can be separately discussed in terms of the effects of the ambient plasma (described by $G(\omega,k)$) and those effects associated with the source charge density. From (1-8) and the fact that $G(t,k)$ vanishes for $t<0$, one finds

$$ikG(\omega,k) = \frac{4\pi}{\varepsilon(z,k)}\Big|_{z=\omega} \quad . \tag{1-10}$$

This states that the reciprocal of the dielectric function defined by a Laplace transform with the complex variable z replaced by the real variable ω is proportional to the Fourier transform of the one dimensional divergence of the Green's function. Strictly speaking, this is different from using $1/\varepsilon(\omega,k)$ (which is the Fourier transform

of $\varepsilon^{-1}(t)$) for the following reason. The $t<0$ behavior of $\varepsilon^{-1}(t,k)$ needed in the Fourier transform depends on what is said about the system during that time. In particular, if there was never any source term then the electric field would not be zero for all $t<0$, based on imagining the plasma system evolving backwards in time starting from a non-trivial $t>0$ solution. Taking (1-2) as defining $\varepsilon^{-1}(t,k)$ for all values of time, then the previous statement implies that, unlike the Green's function, $\varepsilon^{-1}(t,k)$ does not vanish for all $t<0$; hence its Fourier transform differs from that of $ikG(t,k)/4\pi$.

(1-10) is taken to mean that $ikG(\omega,k)$ is expressed by exactly the same function as $4\pi/\varepsilon(z,k)$. But the utility of this function is different when used to study the frequency spectrum, than its use in an instability analysis. The difference is that $G(\omega,k)$ helps to identify features of the electric field power spectrum, not just to determine the asymptotic frequencies.

Applying the results of an earlier discussion concerning the dielectric function to the Green's function, one concludes the Green's function includes physics that describes the response of the plasma plus a uniform frequency spectral contribution corresponding to the delta function in time. Both of these contributions to the power spectrum of the electric field are studied in Chapter 2. To further understand the electric field behavior, Chapter 3 studies the time evolution of the Green's functions. There is also the dependence the electric field has on ρ. Its contribution to the power spectrum is considered for a specific application. Chapter 4 takes as the application the upstream region of the earth's bow shock where both reflected particles and considerable electrostatic wave activity exist.

TWO

Electric Field Frequency Spectrum

2-1. Vlasov Description - The Source-Free Collisionless Plasma

To introduce the equations for the source problem, the Vlasov description of a plasma is first reviewed. The Vlasov equation is based on kinetic theory, and applies to plasmas without any sources for which particle collisions can be neglected [*Nicholson,* 1983]. The plasma can be affected only by externally applied electric and magnetic fields and by the electric and magnetic fields generated by the plasma as a whole. Considering the electrostatic case (curl-free electric and magnetic fields) with no externally applied fields, the Vlasov equation in one spatial dimension can be written (using Gaussian units)

$$\left[\partial_t + v\partial_x + \frac{q_a}{m_a} E(t,x)\partial_v\right] f_a(t,x,v) = 0 \quad , \tag{2-1}$$

where f_a is the particle distribution for species a with mass m_a and charge q_a. This study considers a plasma consisting of electrons (a=e) and protons (a=i). Here x is the spatial coordinate over which f_a and the electric field E vary, and v is the velocity coordinate. The unit vectors for x, v, and E are parallel and point in the same direction. The particle distributions are normalized so that $f_a(t,x,v)\,dx\,dv$ is the particle

number within the infinitesimal phase space "volume" dx dv centered about the phase space point (x,v) at time t.

The Vlasov equation is basically a statement of local particle conservation in phase space. It expresses the fact that the rate of change in the number of particles within an arbitrary control volume in phase space is balanced by the net flux of particles entering or leaving that control volume.

2-2. Vlasov Equation Extended to Include a Source

With a source of plasma capable of injecting particles into the plasma system anywhere in the phase space at any time, the right hand side of (2-1) is not zero. Rather, the flux of particles supplied to the control volume will change the particle number. Defining $\zeta_a(t,x,v)$ as the rate of particle injection of species a per phase "volume" at (x,v), the particle distribution now evolves according to

$$\left[\partial_t + v\partial_x + \frac{q_a}{m_a} E \partial_v\right] f_a = \zeta_a \quad . \tag{2-2}$$

As briefly discussed in Chapter 1, the inhomogeneous term, ζ_a, can represent a variety of physical situations. Besides the conventional case of having a source or sink which is external to the system, this source term can represent the effect of physics not explicitly included in a model of the physical problem. The Introduction mentioned that the effects of particles reflecting from a boundary or a flow obstacle (like the earth's bow shock) on the plasma system can be studied with a source term. This has the benefit of working with a simpler problem than one which describes the reflection process at the boundary. Yet another application might be to study ionization and recombination effects. This affects a plasma system by interchanging

particles of different species, a process which alters the local charge density. By having a source term for each of the particle species, one can include the effects of the ionization process.

f_a in (2-2) has the same meaning as in (2-1). It is the phase space number density for particles of species a which are present in the system at time t. The electric field at time t is determined from the spatial charge density in the system at that time given by Gauss' law

$$\partial_x E(t,x) = \sum_{a=i,e} 4\pi q_a \int dv\, f_a(t,x,v) \quad . \tag{2-3}$$

The range for the velocity integral is from $-\infty$ to $+\infty$. This equation along with (2-2) constitute a non-linear inhomogeneous set of equations which, in principle, one solves for the electric field and the particle distributions in terms of the sources and initial conditions for the particle distributions. An approximation to the equations can be made for situations where the injected particle populations have densities which are significantly less than the background plasma. This is the case in, say, the electron foreshock region of the earth's bow shock, where an electron population, identified as coming from the shock (possibly due to particle reflection at the bow shock), has a number density which is a factor of 100 (or more) times less than the solar wind plasma density [*Klimas,* 1985]. For this case, the source is expected to cause slight changes in the particle distributions, and perturbation theory could adequately describe the plasma evolution. In the next section, the linear problem is introduced.

particles of different species, a process which alters the local charge density. By having a source term for each of the particle species, one can include the effects of the ionization process.

f_a in (2-2) has the same meaning as in (2-1). It is the phase space number density for particles of species a which are present in the system at time t. The electric field at time t is determined from the spatial charge density in the system at that time given by Gauss' law

$$\partial_x E(t,x) = \sum_{a=i,e} 4\pi q_a \int dv\, f_a(t,x,v) \quad . \tag{2-3}$$

The range for the velocity integral is from $-\infty$ to $+\infty$. This equation along with (2-2) constitute a non-linear inhomogeneous set of equations which, in principle, one solves for the electric field and the particle distributions in terms of the sources and initial conditions for the particle distributions. An approximation to the equations can be made for situations where the injected particle populations have densities which are significantly less than the background plasma. This is the case in, say, the electron foreshock region of the earth's bow shock, where an electron population, identified as coming from the shock (possibly due to particle reflection at the bow shock), has a number density which is a factor of 100 (or more) times less than the solar wind plasma density [*Klimas,* 1985]. For this case, the source is expected to cause slight changes in the particle distributions, and perturbation theory could adequately describe the plasma evolution. In the next section, the linear problem is introduced.

2-3. Linear Problem

Separating out the background population F_a, the particle distributions are written $f_a = F_a + f'_a$. Here, f'_a denotes the deviation of the particle distribution function from F_a. The background plasma will be approximated by a Maxwellian velocity distribution

$$F_a(v) = \frac{n}{v_a\sqrt{2\pi}} e^{\frac{-v^2}{2v_a^2}} \tag{2-4}$$

where both species have uniform particle number density n and respective velocity spread v_a. Substitution of f_a into (2-2) and (2-3) results in

$$\left[\partial_t + v\partial_x + \frac{q_a}{m_a} E\partial_v\right] f'_a + \frac{q_a}{m_a} E\partial_v F_a = \zeta_a \tag{2-5a}$$

$$\partial_x E = \sum_a 4\pi q_a \int dv\, f'_a \quad . \tag{2-5b}$$

Assuming the source introduces fluctuations in the particle distribution that are small in comparison to the background, f'_a is taken to be a quantity of first-order in the perturbation scheme. Gauss' law then indicates the electric field is of first-order. Consequently, to first-order, f'_a satisfies

$$(\partial_t + v\partial_x) f'_a + \frac{q_a}{m_a} E\partial_v F_a = \zeta_a \quad . \tag{2-6}$$

For simplicity, the spatial coordinate will be transformed to a Fourier wave number coordinate k. Using $\psi(Y,x)$ to denote any function which depends on x and any other set of independent variables Y (such as t or (t,v)), the transformed function $\psi(Y,k)$ is defined by

$$\psi(Y,x) = \int \frac{dk}{2\pi} e^{ikx} \psi(Y,k) \tag{2-7a}$$

$$\delta(x) = \int \frac{dk}{2\pi} e^{ikx} \quad . \tag{2-7b}$$

Using the Fourier transform definition with this representation of the Dirac delta function $\delta(x)$, (2-6) and (2-5b) can be expressed in terms of the transformed functions

$$(\partial_t + ikv) f'_a(t,k,v) = -\frac{q_a}{m_a} E(t,k) \partial_v F_a + \zeta_a(t,k,v) \tag{2-8a}$$

$$ik\, E(t,k) = \sum_a 4\pi q_a \int dv\, f'_a(t,k,v) \quad . \tag{2-8b}$$

One can solve for f'_a and E using (2-8a) and (2-8b). In regard to measurements, the fluctuations in the particle distribution is difficult to accurately measure. Therefore, the electric field, being most easily measured, will be the only function explicitly determined from the present set of equations. Assuming that fluctuations did not exist in the infinite past, (2-8a) can be solved to find

$$f'_a(t,k,v) = \int_{-\infty}^{t} dt_1\, e^{-ikv(t-t_1)} \{-\frac{q_a}{m_a} E(t_1,k) \partial_v F_a + \zeta_a(t_1,k,v)\} \quad . \tag{2-9}$$

With this relation, (2-8b) becomes (upon performing the velocity integral containing F_a)

$$ik\, E(t,k) + ik \int_{-\infty}^{t} dt_1\, E(t_1,k) K(t-t_1,k) = 4\pi \rho(t,k) \tag{2-10}$$

where

$$K(t,k) = \sum_a \omega_a^2 t\, e^{\frac{-1}{2} k^2 v_a^2 t^2} \tag{2-11}$$

$$\rho(t,k) = \sum_a q_a \iint dt_1\, dv\, \theta(t-t_1)\, e^{-ikv(t-t_1)}\, \zeta_a(t_1,k,v) \quad . \tag{2-12}$$

The step function $\theta(t)$ was introduced in the definition of ρ to allow the integration to range over all time. $\omega_a^2 = 4\pi e^2 n/m_a$ is the square of the plasma frequency for species a (e is the charge magnitude).

Two types of charge density terms are evident from Gauss' law in the form of (2-10). ρ is the spatial charge density of particles coming from the source. The other type involves K convolved in time with the electric field. Such terms account for variations in the charge density due to the electric field accelerating the background plasma. The electric field of these two types of charge density are, respectively, the applied and induced fields discussed in the Introduction. To find the solution to (2-10) for a general applied charge density ρ, it is appropriate to express the electric field in terms of an integral. As presented in the Introduction by (1-5),

$$E(t,k) = \int dt' G(t-t',k)\,\rho(t',k) \quad . \tag{2-13}$$

By requiring the Green's function $G(t-t',k)$ to satisfy

$$ik\,G(t-t',k)+ik\int dt_1 G(t_1-t',k)\,\theta(t-t_1)K(t-t_1,k) = 4\pi\,\delta(t-t') \tag{2-14}$$

the electric field given by (2-13) obeys (2-10). The significance of the Green's function is determined by noting that the inhomogeneous term in (2-14) is the spatial Fourier transform of $4\pi\,\delta(t-t')\,\delta(x-x')$. Therefore, the Green's function is proportional to the electric field produced in a plasma by a uniform sheet of charge located at x' with a surface charge density that varies in time as $\delta(t-t')$. And the electric field for an arbitrary ρ, expressed by (2-13), can be viewed as the resultant field for an infinite number of sheets of charge, with $\rho(t',x')$ specifying the surface charge densities of the sheets. This perspective is more apparent from the inverse transform of (2-13)

$$E(t,x) = \iint dt'dx' G(t-t',x-x')\,\rho(t',x')$$

which explicitly shows the sum over all configurations of the ''sheets''. This perspective will be useful in understanding the results. Specifically, once having explained the Green's function behavior, the effects of a particular applied charge density are understood through summing over the ''sheet'' contributions. Basic

features of the resulting electric field can be determined by studying the Green's function. This analysis will be presented in the following section.

2-4. Electric Frequency Spectrum - The Green's Function Contribution

To study the frequency features of the electric field spectrum, a Fourier transform on the time dependence will be performed. Using ω as the transform variable, the Fourier transform of the Green's function is given by

$$G(t-t',k) = \int \frac{d\omega}{2\pi} e^{-i\omega(t-t')} G(\omega,k) \tag{2-15}$$

where the Fourier transform of the delta function is:

$$\delta(t-t') = \int \frac{d\omega}{2\pi} e^{-i\omega(t-t')} \quad .$$

The convolution integrals appearing in (2-13) and (2-14) can be readily transformed to find

$$E(\omega,k) = G(\omega,k)\,\rho\,(\omega,k) \tag{2-16}$$

$$G(\omega,k) = \frac{4\pi}{ik}\frac{1}{1+\tilde{K}\,(\omega,k)} \tag{2-17}$$

where

$$\tilde{K}(\omega,k) = \int dt\, e^{i\omega t}\theta(t)K\,(t,k) \quad . \tag{2-18}$$

The relationship between the Green's function and the dielectric function ε was derived in the Introduction. This relationship in the form of (1-10) can be verified by recalling that the dielectric function is [*Fried and Culler*, 1963]:

$$\varepsilon(z,k) = 1+\tilde{K}(z,k) \tag{2-19}$$

with z being a complex frequency variable. As discussed in Chapter 1, the same function appears in both the Green's function and the dielectric function, but with a

different argument in each case. Whereas the transform coordinate ω of the Green's function is real, the frequency argument of the dielectric function is in general complex. Furthermore, the Green's function in this study will be used in a more general fashion than the usual application of the dielectric function. The most common use of the dielectric function is to determine the electric field frequencies (with corresponding damping rates) in the asymptotic time limit from the roots of ε [*Nicholson,* 1983], whereas the utility of the Green's function is to determine features of the electric field frequency spectrum, without restricting the spectrum to the asymptotic time limit.

Relating $\tilde{K}$ to tabulated functions, it is found to be proportional to the derivative of the plasma dispersion function of real argument [*Fried and Culler,* 1963]. However, to explicitly display the real and imaginary parts of $\tilde{K}$, it is more convenient to introduce the Dawson integral D(y) [*Abramowitz and Stegun,* 1972] defined as

$$D(y) = e^{-y^2}\int_0^y dw\, e^{w^2}$$

where y can take any real value. In what follows, the small and large argument expansions for the Dawson integral are required. For small values of its argument ($y \ll 1$), the exponential functions can be expanded to obtain

$$D(y) \approx y\left(1-\frac{2}{3}y^2\right) \quad .$$

The asymptotic expansion for the Dawson integral [*Fried and Conte,* 1961] is given by

$$2yD(y) \approx 1+\frac{1}{2y^2}+\frac{3}{4y^4} \quad .$$

Introducing $u_a = \omega/(\sqrt{2}|k|v_a)$, $\tilde{K}$ is:

$$\tilde{K}(\omega,k) = \sum_a \frac{\omega_a^2}{kv_a^2}\left\{1-2u_aD(u_a)+i\sqrt{\pi}u_ae^{-u_a^2}\right\} \quad . \tag{2-20}$$

From this expression important symmetry properties can be identified. Noting the real part of $\tilde{K}$ is an even function of u_a and that the imaginary part is an odd function of u_a, the modulus of the Green's function spectrum is an even function of ω. Also, the dependence u_a has on k involves only the absolute magnitude of k. $\tilde{K}$ is therefore an even function of wave number, indicating the Green's function is an odd function of k. This translates into a spatial symmetry property for the Green's function

$$G(t-t',x-x') = -G(t-t',x'-x) \quad .$$

However, to perform the spatial inverse Fourier transform, more needs to be said concerning the factor of $1/ik$ appearing in (2-17). Formally, $1/ik$ is the Fourier transform representation of integration, since ik arises from the Fourier transform of the divergence of the Green's function. Solving for $G(t-t',x-x')$ for a simple case will determine the necessary modification of the factor $1/ik$. It is convenient to consider the particular case of the zero temperature limit. This limit can be easily taken in the time domain from (2-14). After taking two time derivatives of (2-14), the zero temperature Green's function, $G_o(t-t',k)$, is found to obey

$$ik(\partial_t^2+\omega_o^2)G_o(t-t',k) = 4\pi\partial_t^2\delta(t-t') \tag{2-21}$$

with $\omega_o^2=\sum_a\omega_a^2$. Applying the causality condition that the Green's function must vanish for $t<t'$, (2-21) has the solution

$$G_o(t-t',k) = \frac{4\pi}{ik}\left[\delta(t-t') - \omega_o\sin\omega_o(t-t')\right] \quad . \tag{2-22}$$

The factor $1/ik$ appearing in this equation is not sufficiently defined for computing $G(t-t',x-x')$. However, this difficulty can be resolved by recognizing the term involving the delta function is the applied field for the Green's function problem.

Considering the Green's function as the field due to a sheet of charge located at x' with surface charge density varying as $\delta(t-t')$, the applied field would be $2\pi\,\mathrm{sgn}(x-x')\,\delta(t-t')$ as determined from Gauss's law. Here sgn(x) is the *sign* function ($\mathrm{sgn}(x) = 1$ for $x>0$ and $\mathrm{sgn}(x) = -1$ for $x<0$). This indicates $1/ik$ needs to be replaced by $k/i(k^2+\alpha^2)$, where the limit of $\alpha\to 0$ gives the correct inverse transform based on

$$\frac{1}{2}\,\mathrm{sgn}(x) = \lim_{\alpha\to 0}\int \frac{dk}{2\pi i}\,\frac{k}{k^2+\alpha^2}\,e^{ikx} \quad .$$

Consequently,

$$G_o(\omega,k) = \frac{-4\pi ik}{k^2+\alpha^2}\left[1+\frac{\omega_o^2}{\omega^2-\omega_o^2}\right] \tag{2-23}$$

where the limit of α approaching zero is performed when necessary. For later reference, the two terms in (2-23) are identified, respectively, as the applied and induced fields for the Green's function problem. For the general temperature case, one has

$$G(\omega,k) = \frac{-4\pi ik}{k^2+\alpha^2}\,\frac{1}{\varepsilon(\omega,k)} \tag{2-24}$$

where $\varepsilon(\omega,k)$ is taken to mean $\varepsilon(z,k)$ evaluated at $z=\omega$.

2-5. Induced Portion of the Green's Function

At the end of the last section it was shown that the induced portion of the Green's function for the zero temperature plasma can be separated from the applied field. This section will emphasize the induced portion of the Green's function for arbitrary kv_a. Analogous to (2-23), one would write for the general case

$$G(\omega,k) = \frac{-4\pi ik}{k^2+\alpha^2}+g(\omega,k) \tag{2-25}$$

with $g(\omega,k)$ being the induced contribution to the Green's function. Using (2-24) to

express g in terms of ε, one finds

$$g(\omega,k) = \frac{-4\pi ik}{k^2+\alpha^2}\, h(\omega,k) \qquad (2\text{-}26)$$

where

$$h(\omega,k) = \frac{1}{\varepsilon(\omega,k)} - 1 \quad . \qquad (2\text{-}27)$$

The relevance of $g(\omega,k)$ to observations should be established. Specifically, $g(\omega,k)$ is the induced contribution to the Green's function frequency spectrum associated with the wave number k. However, the process of making observations does not single out a particular wave number. Measurements are more accurately described as being made at a point x in space, and the electric field frequency spectrum at that point, $E(\omega,x)$, would be meaningful. $g(\omega,k)$ appears in $E(\omega,x)$ through the inverse transform of (2-16), with $g(\omega,k)e^{ikx}\rho(\omega,k)$ as a term in a sum over k contributing to the induced electric field. Therefore, much can be understood about the frequency spectrum of the induced field at a point x by studying the dependence $g(\omega,k)$ has on the wave number. The other factor, $\rho(\omega,k)e^{ikx}$, can be thought of as being a weighting function for the sum over k. For example, if $\rho(\omega,k)$ were proportional to $\delta(k-k_o)$, the induced field would be proportional to $g(\omega,k_o)e^{ik_ox}$, where only the wave number k_o gives a non-zero contribution. In addition to this role of selecting the important k values, ρ also has frequency dependence.

The induced electric field $e(\omega,x)$ is related to $g(\omega,k)$ by

$$e(\omega,x) = \int \frac{dk}{2\pi} e^{ikx} g(\omega,k)\, \rho(\omega,k) \quad . \qquad (2\text{-}28)$$

This equation is useful in identifying basic features of the induced electric field frequency spectrum $e(\omega,x)$, since it provides a framework for discussing the induced por-

tion of the Green's function and the source term separately. The remainder of this chapter will focus on the behavior of the induced portion of the Green's function by studying $h(\omega,k)$ of (2-26), which avoids placing undue significance on the spectrum when k is near zero. One can assign a significance to $h(\omega,k)$ by noting that it is proportional to $ikg(\omega,k)$ (for $\alpha\rightarrow 0$) from (2-26). Since $ikg(\omega,k)$ is the Fourier transform of the divergence of the induced Green's function, $h(\omega,k)$ is proportional to the charge density induced in the background plasma for the Green's function problem.

Basic features of $h(\omega,k)$ can be established by applying some known properties about the dielectric function. As is well-known, weakly damped frequencies are determined from the roots of $\varepsilon(z,k)$. These roots correspond to peaks in $h(\omega,k)$, since $\varepsilon(\omega,k)$ then approaches zero for ω nearly equal to the real part of z_o (where $\varepsilon(z_o,k) = 0$ for $\text{Im } z_o \ll \text{Re } z_o$). To analytically see how the weakly damped roots of the dielectric function relate to the frequency spectrum of $h(\omega,k)$, the high and intermediate frequency limits will be examined.

a. The High Frequency Limit ($u_a^2 \gg 1$)

An interesting limit arises when one considers the frequency spectrum of the induced portion of the Green's function for large values of ω ($u_a^2 \gg 1$). Using the asymptotic expansion for the Dawson integral, $\varepsilon(\omega,k)$ determined from (2-19) becomes

$$\varepsilon = 1+\sum_a \left[-\frac{\omega_a^2}{\omega^2}\left[1+3\frac{k^2v_a^2}{\omega^2}\right]+i\sqrt{\pi}\frac{\omega_a^2}{k^2v_a^2}u_a e^{-u_a^2}\right] \quad . \tag{2-29}$$

Since ε approaches 1 in the limit of $\omega\rightarrow\infty$, $h(\omega,k)$ vanishes in the infinite frequency limit. The asymptotic behavior of $h(\omega,k)$ is equal to the zero temperature expression given by the second term of (2-23), indicating the asymptotic frequency behavior is

insensitive to the plasma temperature.

In this high frequency limit it is also possible for a peak to appear in the h frequency spectrum. This is evident from observing from (2-29) that ε is able to achieve small values for frequencies within the range of validity of the approximation if kv_a is small. The constraint on kv_a arises from maintaining the high frequency approximation ($u_a^2 \gg 1$) and allowing the range for the values of ω to include the frequency that makes the real part of (2-29) vanish (when $\omega \approx \omega_e$). This results in requiring $2k^2v_a^2 \ll \omega_e^2$. For such a combination of values of wave number and thermal speeds, $h(\omega,k)$ is exponentially large at the peak frequency ω_{peak}, where approximately

$$\omega_{peak}^2 \approx \omega_e^2 \left[1+3\frac{k^2v_e^2}{\omega_e^2}\right] \quad . \tag{2-30}$$

(2-30) is the well-known Langmuir dispersion relation [*Nicholson,* 1983]. The Landau damping rate associated with this frequency appears in the imaginary part of (2-29) and is important for determining the height of the peak, with a small damping rate corresponding to a large peak.

b. The Intermediate Frequency Range for $v_i^2 \ll v_e^2$

Different from the high frequency limit, which always has some range of application, the intermediate frequency case applies only if $v_i^2 \ll v_e^2$. In terms of T_a, the temperature for species a, the squared thermal velocity ratio is $v_i^2/v_e^2=(m_eT_i)/(m_iT_e)$. This ratio is much less than 1 for physical systems in which $T_i \sim T_e$, since $m_e \ll m_i$. One can then speak of an intermediate frequency range given by $2k^2v_i^2 \ll \omega^2 \ll 2k^2v_e^2$. Using the asymptotic expression for terms depending on u_i^2 and the small argument expression for terms depending on u_e^2 in (2-19) yields

$$\varepsilon(\omega,k) \simeq 1-\frac{\omega_i^2}{\omega^2}+\frac{\omega_e^2}{k^2v_e^2}(1-2u_e^2)+i\sqrt{\pi}\left[\frac{\omega_i^2}{k^2v_i^2}u_i e^{-u_i^2}+\frac{\omega_e^2}{k^2v_e^2}u_e(1-u_e^2)\right] \quad . \tag{2-31}$$

To determine if a peak may be present in this frequency range, consider separately the real and the imaginary parts in (2-31). Note that for finite u_e, the imaginary part is not likely to be exponentially small because of its polynomial dependence on u_e. The imaginary part is essential in determining the height of the peak. One therefore expects the peak to be modest in comparison to the pronounced peak which can occur in the high frequency regime for small $k^2v_a^2$ from (2-29). Roughly speaking, the location of the peak in the intermediate frequency range is determined by the frequency value for which the real part of (2-31) vanishes. Using the condition $u_e^2 \ll 1$, the peak frequency is given by

$$\omega_{peak}^2 \simeq \omega_i^2 \frac{k^2\lambda_D^2}{1+k^2\lambda_D^2} \tag{2-32}$$

where λ_D is the Debye length, $\lambda_D = v_e/\omega_e$. This relationship between the frequency peak and wave number is identical to the dispersion relation for the ion-acoustic mode [*Krall and Trivelpiece,* 1973]. Therefore, this frequency peak in the induced portion of the Green's function is the ion-acoustic wave.

A frequency spectrum which meets the requirement $v_i^2 \ll v_e^2$ is expected to display a peak determined from (2-32). In addition, the same Green's function may exhibit a pronounced peak in the high frequency regime, since the condition $2k^2v_a^2 \ll \omega_e^2$ may be compatible with the condition $v_i^2 \ll v_e^2$. But, as mentioned above, the peak in the intermediate frequency range is less pronounced than this high frequency peak. Hence, the high frequency peak dominates the behavior of the induced portion of the Green's function when $v_i^2 \ll v_e^2$ and $2k^2v_a^2 \ll \omega_e^2$.

c. The Spectrum for Arbitrary kv_a

In the limits previously considered, the weakly damped frequencies were shown to be associated with peaks in the spectrum of the induced portion of the Green's function. Now consider arbitrary values of kv_a. There is one immediate effect that can be anticipated from the degree of damping for a given wave number. That is, for plasma parameters which result in waves that are moderately damped, one expects the local maxima to be less pronounced than the peaks previously considered because of enhanced damping. This diminished frequency peak would occur for parameters which are not included in the limiting cases.

The degree to which the limiting cases approximate the exact frequency spectrum is anticipated by reviewing the conditions on which the limits are based. In formulating the various frequency limits, the conditions were always stated by comparing the square u_a^2 to 1 rather than simply $u_a=\omega/|k|v_a$. Therefore, the various limits are applicable for a good portion of a linear frequency scale. For frequency ranges such that u_a is comparable to 1, the limiting cases will be a poor approximation to the exact frequency spectrum.

Figure 2-1 displays $|h|^2$ as a function of positive frequencies determined from (2-27) and (2-19) for the temperature ratio $T_i/T_e=1$, and values of $k^2\lambda_D^2$ ranging from 0.01 to 0.4. From this figure, one can identify the features corresponding to the high frequency limit. There is the feature that all the graphs asymptotically approach the same function as computed in the high frequency limit. Also sharp peaks occur near $\omega=\omega_e$ for the smaller values of $k^2\lambda_D^2$. The shift in the location of the high frequency peaks is accounted for by the thermal correction term given in (2-30).

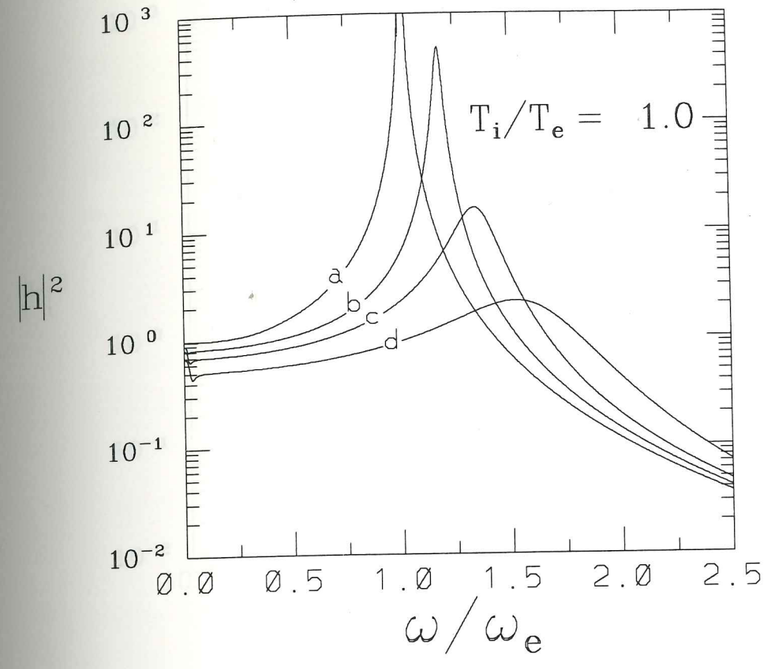

Figure 2-1 $\log_{10}|h(\omega,k)|^2$ versus ω/ω_e (a) $k^2\lambda_D^2 = 0.01$ (b) $k^2\lambda_D^2 = 0.1$ (c) $k^2\lambda_D^2 = 0.2$ (d) $k^2\lambda_D^2 = 0.4$.

Another interesting observation comes from the moderate electron thermal speeds or wave numbers ($k^2\lambda_D^2 = 0.2$ and 0.4). For these values, the low and high frequency ends of the spectrum are much closer in intensity than for smaller $k^2\lambda_D^2$. There is an overall tendency to a broad frequency spectrum. The decrease in the high frequency peak is a result of the appreciable damping that occurs for these thermal speeds.

To study peaks associated with the ion-acoustic wave in comparison to the high frequency peak, Figure 2-2 uses a logarithmic frequency scale and a temperature ratio of T_i/T_e=0.1. In agreement with findings of the two frequency limits, the ion-acoustic

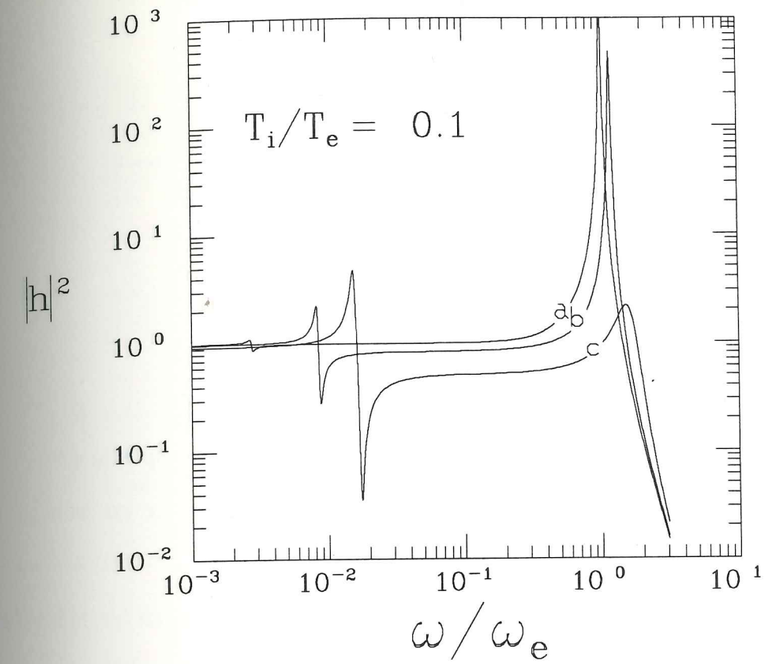

Figure 2-2 $\log_{10}|h(\omega,k)|^2$ versus $\log_{10}(\omega/\omega_e)$ (a) $k^2\lambda_D^2 = 0.01$ (b) $k^2\lambda_D^2 = 0.1$ (c) $k^2\lambda_D^2 = 0.4$.

peaks are less pronounced than the large high frequency peaks. The more pronounced of the ion-acoustic peaks are for the larger values of $k^2\lambda_D^2$, in agreement with (2-31) showing a reduced imaginary part for decreased u_e. The effect of increasing the proton temperature is seen in Figure 2-3 using T_i/T_e=1, where the ion-acoustic peaks are no longer significant. That a small proton to electron temperature ratio yields significant ion-acoustic peaks is predicted from the near-zero behavior of ε in (2-31).

The spectrum weakly depends on the temperature of the proton population except for the low frequencies. This is a consequence of the proton's sluggish

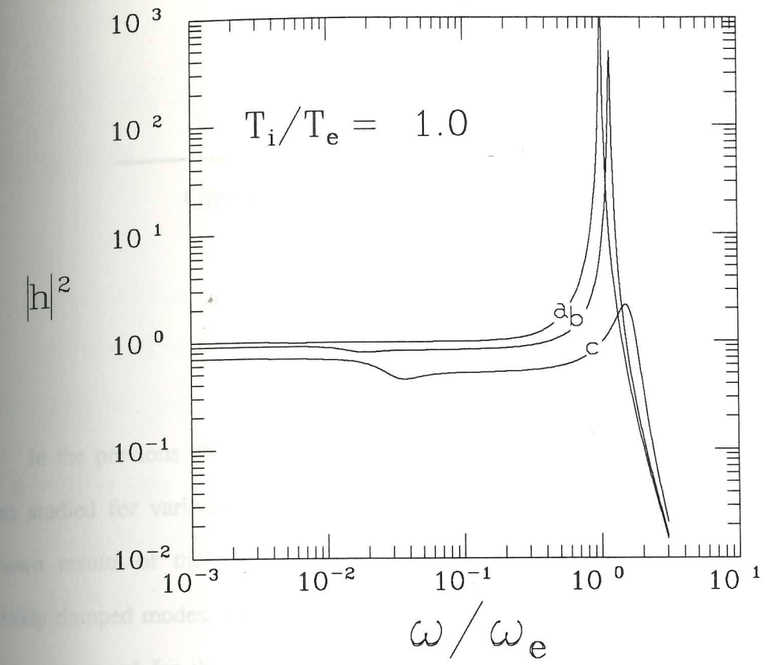

Figure 2-3 $\log_{10}|h(\omega,k)|^2$ versus $\log_{10}(\omega/\omega_e)$ (a) $k^2\lambda_D^2 = 0.01$ (b) $k^2\lambda_D^2 = 0.1$ (c) $k^2\lambda_D^2 = 0.4$.

response to the generated electric field, as can be seen immediately from (2-14), since ω_i^2 is 1836 times smaller than ω_e^2. The proton charge density does not change nearly as fast as that of the electron population. For the same $k^2\lambda_D^2$, the result shown in Figure 2-2 differs from Figure 2-3 only in the extremely low frequency end of the graphs. A good portion of the frequency activity is therefore due to the electron population.

Having studied the Fourier transform of the induced portion of the Green's function, Chapter 3 considers its temporal behavior.

THREE

Green's Function - The Temporal Behavior

In the previous chapter the frequency Fourier transform of the Green's function was studied for various wave numbers. Its features were compared with the well-known results of the Landau problem. For wave numbers corresponding to the weakly damped modes, sharp frequency peaks exist, and these peaks are considerably less pronounced for the moderately damped modes. This chapter will study the frequency spectral behavior for finite time intervals. It will be established that the frequency characteristics change in time, as seen from comparing the short time limit with the asymptotic time limit of the Green's function.

3-1. Temporal Behavior

In the time domain, the relationship between the Green's function and the induced portion of the Green's function obtained from (2-25) is:

$$G(t-t',k) = \frac{-4\pi ik}{k^2+\alpha^2}\left[\delta(t-t')+h(t-t',k)\right] \tag{3-1}$$

where h, representing the induced charge density, is used instead of g. Substituting (3-1) into (2-14), h must satisfy

$$h(t-t',k)+\int_{-\infty}^{t} dt_1 h(t_1-t',k)K(t-t_1,k)=-\theta(t-t')K(t-t',k) \quad . \tag{3-2}$$

This equation can be simplified using the causal relation that exists between the source $\delta(t-t')$ and the response $h(t-t',k)$. Since $h(t-t',k)$ is zero for $t<t'$, (3-2) reduces to

$$h(\tau,k)+\int_{0}^{\tau} d\tau_1 h(\tau-\tau_1,k)K(\tau_1,k) = -K(\tau,k) \quad , \quad \tau>0 \tag{3-3}$$

where the substitution $\tau=t-t'$, and a change of integration variable has been made. The following subsections will solve (3-3) for three different time regimes: short, intermediate and long (asymptotic).

a. Short-Time Limit

Consider the time interval $0<\tau<T$ such that $k^2v_a^2T^2\ll 2$. This defines a short-time period where $K(\tau,k)$ is approximately equal to $\omega_o^2\tau$, yielding as a solution to (3-3)

$$h(\tau,k) = -\omega_o \sin \omega_o\tau \tag{3-4}$$

with $\omega_o^2=\sum_a \omega_a^2$. This approximation is identically equal to the zero temperature case, since $K(\tau,k)=\omega_o^2\tau$ for $v_a=0$. Thus the Green's function for a given plasma background initially responds at the undamped frequency ω_o independent of the thermal speed. This agrees with a result obtained by *Weitzner* [1964], where the Laplace transform representation was used.

b. Asymptotic Time Limit

In Chapters 1 and 2, it was discussed that the Green's function can be approximated by frequencies given by the complex roots of the dispersion function in the asymptotic time limit, based on knowledge of the Landau problem. Here, this will be confirmed and an order of magnitude estimate will be made as to when the

asymptotic time limit applies.

The procedure which will be employed is akin to that used in determining the normal modes for a linear homogeneous differential equation with constant coefficients. This method entails saying $h(\tau,k)$ is a sum of terms that vary as $Ae^{-iz\tau}$, with z as a complex frequency to be determined, and A a constant in time. There is the further aim to determine when this functional form approximately satisfies (3-3). The constraint on the time is determined by requiring (3-3) to be approximately homogeneous and for the frequency z to be fairly insensitive to the actual value of τ. Both of these requirements are satisfied by τ such that $\frac{1}{2}k^2v_a^2\tau^2 \gg 1$. With this restriction and by making the prescribed substitution for $h(\tau,k)$ into (3-3), one finds that the complex frequency is determined from

$$1+\int_0^\infty dt\, e^{izt}K(t,k) = 0 \qquad (3\text{-}5)$$

or simply,

$$\varepsilon(z,k) = 0 \quad . \qquad (3\text{-}6)$$

This expression can readily be solved for the weakly damped modes discussed in Chapter 2. The weakly damped modes are defined by $\omega_R \gg \gamma$ with $z=\omega_R+i\gamma$. Following *Nicholson* [1983], the approximate solution to (3-6) can be found by expanding this equation to first-order in γ and setting its real and imaginary parts to zero. The Langmuir mode has the solution

$$z \approx \omega_e(1+\frac{3}{2}k^2\lambda_D^2) - i\left[\frac{\pi}{8}\right]^{\frac{1}{2}}\sum_a \frac{\omega_a^2}{k^2v_a^2}\frac{\omega_e^2}{|k|v_a}e^{\frac{-\omega_e^2}{2k^2v_a^2}} \qquad (3\text{-}7)$$

for $k^2v_a^2 \ll 2\omega_e^2$. And for the ion-acoustic mode, one has

$$\omega_R \simeq \omega_i^2 \frac{k^2\lambda_D^2}{1+k^2\lambda_D^2} \tag{3-8}$$

$$\gamma \simeq -\left[\frac{\pi}{8}\right]^{\frac{1}{2}} \omega_R^2 \sum_a \frac{\omega_a^2}{|k|^3 v_a^3} e^{\frac{-\omega_R^2}{2k^2v_a^2}}$$

assuming $v_e^2 \gg v_i^2$.

From comparing the results of the short-time limit in (3-4) to the results of the asymptotic time limit in (3-7) and (3-8), it is concluded that the frequency characteristics of the Green's function must vary in time. For a given wave number, the Green's function oscillates at the plasma frequency ω_0 for times $\tau^2 \ll 2k^{-2}v_a^{-2}$. In particular, the Green's function does not experience damping in the short-time limit. But, as the system progresses, damping and a shift in oscillation frequency of the high frequency peak occurs as confirmed by examining the asymptotic limit.

c. Intermediate Time Range for $v_i^2 \ll v_e^2$

Consider an intermediate time interval $2/k^2v_e^2 \ll \tau \ll 2/k^2v_i^2$, which exists for $v_i^2 \ll v_e^2$. From (2-11), the approximate expression for $K(\tau,k)$ is

$$K(\tau,k) \simeq \omega_e^2 \tau e^{\frac{-1}{2}k^2v_e^2\tau^2} + \omega_i^2\tau \quad .$$

Note that the ion thermal effects are negligible in this limit. This is contrasted to the short-time limit where both electron and ion thermal effects are negligible, and to the asymptotic limit where the thermal effects of both species are significant.

Setting the above expression for $K(\tau,k)$ into (3-3), and taking two derivatives with respect to τ, $h(\tau,k)$ approximately obeys

$$\partial_\tau^2 h(\tau,k) + \omega_i^2 h(\tau,k) + \omega_e^2 \int_0^\tau d\tau_1 \, \partial_\tau^2 h(\tau-\tau_1,k)\tau_1 e^{\frac{-1}{2}k^2v_e^2\tau_1^2} \simeq 0$$

subject to the initial conditions $h(0,k)=0$, and $\partial_\tau h(0,k) \simeq -\omega_i^2$. Then, analogous to the

procedure used to solve the asymptotic time limit case, $h(\tau,k)$ for the intermediate time range is shown to consist of frequencies z which must satisfy

$$1-\frac{\omega_i^2}{z^2}+\omega_e^2\int_0^\infty d\tau\, e^{-iz\tau}\,\tau\, e^{\frac{-1}{2}k^2v_e^2\tau^2} = 0 \quad . \tag{3-9}$$

This relation, as well expected, is $\varepsilon(z,k)=0$ in the limit of $v_i\to 0$. The result means that the ion-acoustic waves are damped only by the electron thermal effects for the intermediate-time range.

d. Finite Time Behavior - The Time Power Series

The inverse Fourier transform of (2-24) provides an integral expression for $G(\tau,k)$

$$G(\tau,k) = \frac{-4\pi ik}{k^2+\alpha^2}\int\frac{d\omega}{2\pi}\frac{e^{-i\omega\tau}}{\varepsilon(\omega,k)} \quad . \tag{3-10}$$

However, this is a formidable integral to perform. One might try relating this integral to the contour integral of $\exp(-iz\tau)/\varepsilon(z,k)$ along a closed contour consisting of the real axis from $-R$ to $+R$ and a semicircle of radius R in the lower half plane where the limit $R\to\infty$ is taken. This enables one to apply Cauchy's integral formula which expresses the integral in terms of the residues of the integrand. However, it is complicated to determine the zeros and the order of the zeros of $\varepsilon(z,k)$. From (2-18), $\tilde{K}(\omega,k)$ can be expanded in a power series in ω, which from (2-19) shows $\varepsilon(z,k)$ is a power series in z with an infinite number of terms. Consequently, ε may well have an infinite number of roots of various orders, and the method of residues becomes impractical for studying the finite time behavior without a good knowledge of the pole structure of ε. Therefore, a different means of solution will be used. Another way of finding the temporal behavior is to solve (3-3) by expressing $h(\tau,k)$ as a power

series in τ. Unfortunately, this method suffers from truncation error [*Dahlquist and Björck*, 1974], meaning the power series solution is of limited utility. Nonetheless, the solution will be instructive.

It proves convenient to introduce an intermediate function, $q(\tau,k)$, defined by

$$q(\tau,k) = \int_0^\tau d\tau_1 h(\tau_1,k) + q(0,k) \tag{3-11}$$

where the τ=0 value $q(0,k)$ is as yet unspecified. With $h(\tau,k) = \partial_\tau q$, (3-3) may be rewritten as

$$\partial_\tau \left\{ q(\tau,k) + \int_0^\tau d\tau q(\tau-\tau_1,k) K(\tau_1,k) \right\} = \left[q(0,k) - 1 \right] K(\tau,k) \quad . \tag{3-12}$$

With the judicious choice of $q(0,k)=1$, (3-12) integrates to

$$q(\tau,k) + \int_0^\tau d\tau q(\tau-\tau_1,k) K(\tau_1,k) = 1 \quad . \tag{3-13}$$

$K(\tau,k)$ can readily be expanded in a power series from (2-11), yielding

$$K(\tau,k) = \sum_{m=0}^{\infty} \sum_a \omega_a^2 \frac{1}{m!} \left[\frac{-k^2 v_a^2}{2} \right]^m \tau^{2m+1} \quad . \tag{3-14}$$

From (3-13) and the fact that $K(\tau,k)$ is a series involving only odd powers of τ, $q(\tau,k)$ has the form

$$q(\tau,k) = \sum_{m=0}^{\infty} \xi_m (\omega_o \tau)^{2m} \tag{3-15}$$

as there are no odd power terms. Substituting (3-15) and (3-14) into (3-13) yields the relation

$$\xi_{n+1} = -\sum_{m=0}^{n} \sum_a \frac{\omega_a^2}{\omega_o^2} \left[\frac{-k^2 v_a}{2\omega_o^2} \right]^m \frac{1}{m!} B(2m+2, 2n-2m+1) \xi_{n-m} \quad n>0 \tag{3-16}$$

where $\xi_0=1$ and $B(j,m)$ is the *beta function* [*Morse and Feshbach*, 1953]. Using the relation

$$B(j,m) = \frac{1}{j}\frac{1}{\begin{bmatrix} j+m-1 \\ j \end{bmatrix}}$$

where the binomial coefficients are denoted by

$$\begin{bmatrix} j \\ m \end{bmatrix} = \frac{j!}{m!(j-m)!} \quad ,$$

(3-16) then becomes

$$\xi_{n+1}=\frac{-1}{2}\sum_{m=0}^{n}\sum_{a}\frac{\omega_a^2}{\omega_o^2}\left[\frac{-k^2v_a^2}{2\omega_o^2}\right]^m \frac{1}{(m+1)!}\begin{bmatrix} 2n+2 \\ 2m+2 \end{bmatrix}^{-1}\xi_{n-m} \quad n>0 \quad . \tag{3-17}$$

From (3-17), the coefficients $\{\xi_i\}$ can be determined sequentially, and the power series solution would be applicable for times $\omega_o^2\tau^2<R$. Here,R is the radius of convergence of the series [*Morse and Feshbach,* 1953], and can be calculated from

$$R = \lim_{n\to\infty}\frac{|\xi_n|}{|\xi_{n+1}|} \quad . \tag{3-18}$$

Unfortunately, the recursion relation in the form of (3-17) does not lend itself to direct computation of R. It will be determined by finding a bound for the coefficients under a restriction on k. Define another set of coefficients $\{\beta_i\}$ by

$$\xi_n = \frac{(-1)^n}{n!}\beta_n \quad . \tag{3-19}$$

This relation substituted into (3-17) determines the recursion relation

$$\beta_{n+1}=\frac{1}{2}\sum_{m=0}^{n}\sum_{a}\frac{\omega_a^2}{\omega_o^2}\left[\frac{k^2v_a^2}{2\omega_o^2}\right]^m \begin{bmatrix} n+2 \\ m+1 \end{bmatrix}\begin{bmatrix} 2n+2 \\ 2m+2 \end{bmatrix}^{-1}\beta_{n-m} \quad n>0 \tag{3-20}$$

where $\beta_0=1$. It will now be proven that $\beta_n\geq\beta_{n+1}$ for restricted values of $k^2v_a^2$. First note from (3-20) that $\beta_1=1/2$. Hence, consider the difference of two sequential coefficients

$$\beta_n-\beta_{n+1} = \frac{1}{2}\sum_{a}\frac{\omega_a^2}{\omega_o^2}\left[\sum_{m=0}^{n-2}\left[\frac{k^2v_a^2}{2\omega_o^2}\right]^m \begin{bmatrix} n \\ m+1 \end{bmatrix}\begin{bmatrix} 2n \\ 2m+2 \end{bmatrix}^{-1}\left\{\beta_{n-m-1}-\frac{2n-2m-1}{2n+1}\beta_{n-m}\right\}\right.$$

$$+\frac{1}{2}\left[\frac{k^2v_a^2}{2\omega_o^2}\right]^{n-1}\left\{2-\frac{1}{2n+1}-\frac{k^2v_a^2}{\omega_o^2}\right\}\Bigg] \qquad n>0 \quad . \tag{3-21}$$

In writing (3-21), the summation convention that $\sum_{m=0}^{N} A_m = 0$ for $N<0$ is adopted. From (3-21), one can ensure that $\beta_n \geq \beta_{n+1}$ for all n by choosing $k^2v_a^2$ so that $\beta_1 \geq \beta_2$. This imposes the constraint $k^2v_a^2/\omega_o^2 \leq 5/3$, which is not a severe limitation. Under this restriction, the radius of convergence is readily found from (3-18) and (3-19) to be infinite. In other words, the power series converges for all values of τ.

In Figure 3-1, $h(\tau,k)$ is plotted as a function of τ for $v_i=0$. The various curves correspond to different values of $k^2\lambda_D^2$. The curves which are terminated before $\omega_o\tau/2\pi=5$ (5 plasma periods) were done so to avoid the eventual instability due to

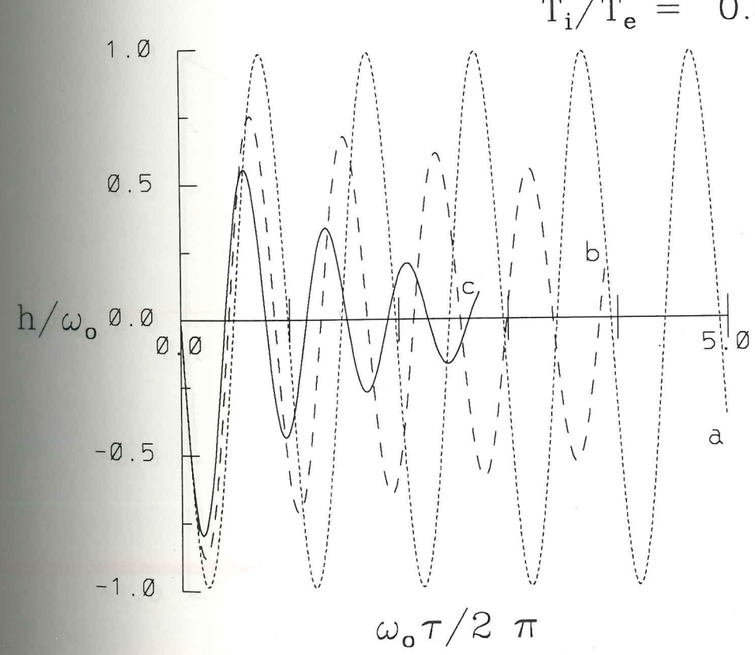

Figure 3-1 $h(\tau,k)/\omega_o$ versus $\omega_o\tau/2\pi$ (a)$k^2\lambda_D^2 = 0.01$ (b)$k^2\lambda_D^2 = 0.1$ (c)$k^2\lambda_D^2 = 0.2$.

truncation error in evaluating the power series. Figure 3-1a ($k^2\lambda_D^2=0.01$) shows slight damping with an average frequency of slightly higher than the plasma frequency ω_o. For Figure 3-1b and Figure 3-1c (increased $k^2\lambda_D^2$) the curves show noticeable damping and higher frequencies. These results are in agreement with the features determined from the short and asymptotic time limits with $\tau^2=2/k^2\lambda_D^2$ as the relevant scale time for distinguishing the two limits. In particular, all the curves start off approximately equal, as expected from the short-time limit.

As an additional comparison, Figure 3-2 shows both $h(\tau,k)$ and the envelope of the asymptotic solution, $e^{\gamma\tau}$, with γ given by the imaginary part of (3-7), for $k^2\lambda_D^2=0.1$

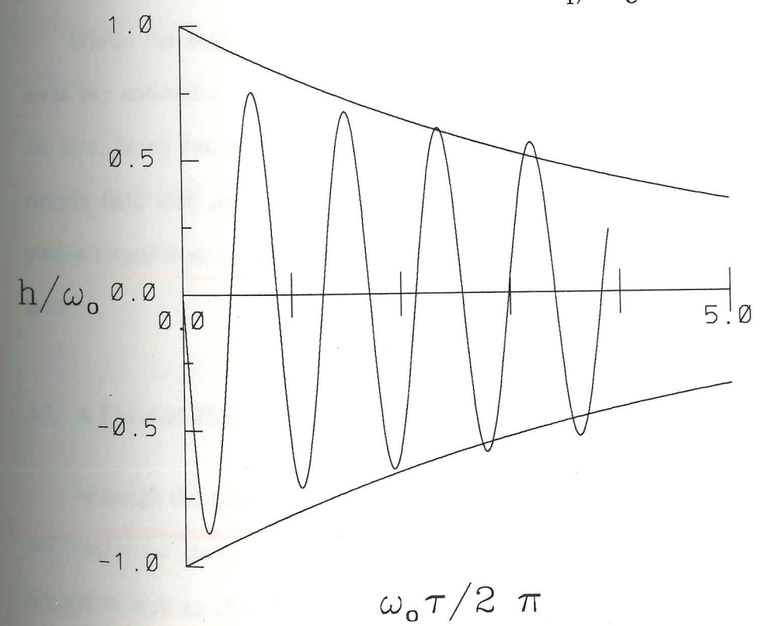

Figure 3-2 $h(\tau,k)/\omega_o$ versus $\omega_o\tau/2\pi$ shown with the envelope of the asymptotic solution for $k^2\lambda_D^2 = 0.1$.

applying a variation of this technique.

The time power series of the previous section can be derived formally by expanding in a time ordering parameter λ. This is accomplished by replacing every occurrence of τ by $\lambda\tau$ (and similarly for the integration time τ_1) in (3-13), which amounts to rescaling the measure of time. One solves for $q(\lambda\tau,k)$ in the form

$$q(\lambda\tau,k) = \sum_{n=1}^{\infty} \nu_n(\tau,k)\lambda^{2n+1} \tag{3-22}$$

where the desired result $q(\tau,k)$ is obtained by setting $\lambda=1$. The function $\nu_n(\tau,k)$, determined from (3-13), depends on τ^{2n+1}, since $\nu_n(\tau,k)$ has the coefficient λ^{2n+1} in (3-22). This establishes the expansion as a power series in τ.

Since q also depends on k, the general procedure of expanding the series in terms of an ordering parameter suggests ordering in terms of the wave number. The intention is to obtain a physical description of the Green's function response. Consequently, the form rather than the quantitative result will be emphasized. Specifically, for the ordering in wave number defined by

$$q(\tau,\lambda k) = \sum_{n=0}^{\infty} \mu_n \lambda^{2n} \quad , \tag{3-23}$$

the form of the function $\mu_n(\tau,k)$ is desired. (3-23) involves only even powers of λ because (3-13) indicates $q(\tau,\lambda k)$ has the same λ dependence as $K(\tau,\lambda k)$. Substituting the power series in λ for q and K into (3-13) leads to

$$\mu_n(\tau,k)+\omega_o^2\int_0^{\tau} d\tau_1 \mu_n(\tau_1,k)(\tau-\tau_1) = -\sum_{m=1}^{n} A_m \int_0^{\tau} d\tau_1 \mu_{n-m}(\tau_1,k)(\tau-\tau_1)^{2m+1} \quad n>0 \tag{3-24}$$

where

$$\mu_0(\tau,k) = \cos\omega_o\tau$$

and

$$A_m = \sum_a \omega_a^2 \frac{1}{m!} \left[\frac{-k^2 v_a^2}{2}\right]^m \quad .$$

The integrals in (3-24) can be eliminated by taking 2n+2 derivatives with respect to τ. The form of the solution for these differential inhomogeneous equations is more easily arrived at by imposing a limiting process. In particular, replace ω_o appearing on the left side of (3-24) with $\omega_{n\alpha}$ defined by

$$\omega_{n\alpha}^2 = \omega_o^2 + n^2\alpha^2 \quad , \tag{3-25}$$

where in the limit $\alpha \to 0$ the desired equations result. Taking 2n+2 derivatives of the modified (3-24) one obtains

$$\left[\partial_\tau^2 + \omega_{n\alpha}^2\right] Y_n(\tau,k) = -\sum_{m=1}^{n} (2m+1)! A_m Y_{n-m}(\tau,k) \quad , n>0 \tag{3-26}$$

where $Y_n = \partial_\tau^{2n} \mu_n$. Note that $Y_0 = \mu_0$.

It is necessary to specify the initial conditions for these differential equations. These are derived from evaluating (3-24) and its derivatives at $\tau = 0$. It follows that the initial conditions are

$$\partial_\tau^M \mu_n(0,k) = 0 \qquad M<2n+2, \; n>0 \quad . \tag{3-27}$$

Subject to these initial conditions one can solve (3-26) for $\mu_n(\tau,k)$. Consider as an intermediate step determining Y_{2n}, which has as initial conditions $Y_n(0,k) = \partial_\tau Y_n(0,k) = 0$. It becomes clear that in conjunction with $Y_0(\tau,k) = \cos\omega_o\tau$, the solution of (3-26) has the form

$$Y_n = \sum_{m=0}^{n} b_{n,m} \cos \omega_{m\alpha}\tau \quad . \tag{3-28}$$

Integrating 2n times, one has

$$\mu_n(\tau,k) = \sum_{m=0}^{n-1}\left[\left[\frac{-1}{\omega_{m\alpha}^2}\right]^n b_{n,m}\cos\omega_{m\alpha}\tau + c_{n,m}\tau^{2m}\right] + \left[\frac{-1}{\omega_{n\alpha}^2}\right]^n b_{n,n}\cos\omega_{n\alpha}\tau \qquad (3\text{-}29)$$

where the limit $\alpha\to 0$ is understood. The integration constants associated with the odd powers of τ are zero based on the initial conditions for the odd derivatives of μ_n. The integration constants $c_{n,m}$ are determined from the remaining initial conditions.

With the integration constants chosen to satisfy the initial conditions (3-27), it follows that the lowest order term in a τ expansion of $\mu_n(\tau,k)$ varies as τ^{2n}. This means the functions $\{\mu_i\}$ contribute sequentially in time. In other words, as the plasma response progresses, more terms in the λ expansion become significant for some specified measuring accuracy. The response consists of oscillations which are infinitesimally close to the frequency ω_o, and an additional portion associated with the integration constants. These facts motivate a physical explanation of the results by visualizing the motion of the plasma particles. To facilitate this, consider the application of an impulsive electric field that varies sinusoidally in space. Specifically, say that the charge density that gives rise to the applied field varies as $\cos k_o x\,\delta(t-t_o)$, or

$$\rho(t,k) = 2\pi B\delta(t-t_o)\left\{\delta(k-k_o)+\delta(k+k_o)\right\} \qquad (3\text{-}30)$$

with B, t_o and k_o as constants. Substituting (3-30) into the appropriate transformation of (2-28), the induced electric field, $e(t,x)$, is

$$e(t,x) = \frac{4\pi B}{k_o}h(t-t_o,k_o)\sin k_o x \quad . \qquad (3\text{-}31)$$

For the case of a zero temperature plasma, only the term μ_o contributes to (3-31), yielding $e(t,x) = -(4\pi B/k_o)\omega_o \sin\omega_o(t-t_o)\sin k_o x$, $t>t_o$. This result is particularly easy to understand in terms of the particle motion. First, the minus sign is in accordance with $e(t,x)$ being an induced field. The induced field arises because the applied force,

acting on $t=t_o$, imparts a momentum to the particles which, for $t<t_o$, are all at rest. Subsequently, the system executes oscillations in time because the particles experience a restoring force from the electric field created by the spatially varying charge density of the relocated particles.

A useful perspective to cast the cold plasma result is to regard the particles as being distributed over an infinite number of rigid sheets with constant surface charge density. The distribution process is done by considering the $t<t_o$ configuration of particles. Namely, the electrons and ions at a given point x are assigned to respective electron and ion sheets, and these sheets are uniformly arranged during $t<t_o$. Subsequent to the application of the impulse, the density variations are accounted for by the relative positioning of the sheets. It is evident that a particle never leaves its sheet. In other words, a particle always remains with the same group of particles. The oscillation is visualized by the sheets moving back and forth across the nearest electric field node. This picture emphasizes the salient points that lead to an understanding of a thermalized plasma.

For $v_a \neq 0$, the particles at a given point x do not all have the same velocity, since the particles have a Maxwellian velocity distribution. Therefore, if one were to impose the rigid sheet description, a given sheet will be comprised of different particles as time progresses. Furthermore, the charge density of a sheet, in general, varies in time. The sheets can be uniformly spaced for $t<t_o$, during which time the surface charge densities are constant, and they superimpose to give a zero net charge. However, the thermalized particles move to different sheets, even though the charge densities are constant during this time. And for $t>t_o$, both the charge density and the

location of the sheets vary.

The differences between the sheet descriptions for cold and thermalized plasmas suggest the wave number expansion, in effect, accounts for the adjustment of the sheet locations and charge densities as particles of even higher velocities become significant. The qualitative features can be readily identified. For times immediately following t_o, the response is dominated by $\partial_{\tau}\mu_0$, the cold plasma response, because the particles which were initially at rest dominate in number and travel the least distance for the given infinitesimal time period. In traveling the least distance these particles see the induced electric field evolve the least, whereas the thermalized particles, in traveling longer distances, see the induced electric field vary in a more complex fashion. This complexity corresponds to higher order corrections of the field. The terms of the wave number ordering, in succession, take into account the adjustment in the electric field due to particles of progressively higher velocity and due to corrections in motion of the particles of lesser velocity.

With this acquired understanding, the overall electric field damping which the plasma experiences is explained by the particles traveling over different lengths. In general, the particles in responding to the developing electric field attempts to cancel the field out, but the inertia of the particles cause the field to persist. The damping is due to the particles canceling the field in the overlapping regions that span across the spatial nodes. This has the effect of redistributing the original induced charge density over all space to an eventual zero charge density configuration. A characteristic time for this redistribution to be significant is $2\pi/k_o v_a$ which roughly corresponds to the time it takes for the thermalized particles to travel across the spatial scale. This esti-

mate is consistent with the analytical study of the various time limits, which identifies $k^2v_a^2T^2/2$ as determining which limit is applicable.

3-3. Discrete Power Spectrum

In summary, the Green's function has been studied in various forms. Chapter 2 emphasized the frequency Fourier transform, which was helpful in putting the well-known results of the Landau problem in perspective with the source problem. The general evolution of the Green's function was at issue in the previous sections of this chapter, where it was shown that the frequency varies as time progresses. There remains one more computation to perform for the purpose of comparison with reported space plasma observations. Measurements of the electric field are made by determining its amplitude for a given frequency band. Therefore, the calculation of the discrete frequency Fourier transform is quantitatively relevant, since the transform coefficients are the amplitudes of the corresponding frequency bands.

A discrete Fourier transform requires specifying a time period, $T_A \le t \le T_A+T$, over which the transform coefficients are computed. The duration of the observation, T, is large in comparison to the plasma period to give good frequency resolution. This rules out employing the power series solution, as it is not practical for large times. Instead, matrix relations for the field amplitude (the transform coefficient) will be derived, and then solved by computer.

For a finite observation period $T_A \le t \le T_A+T$, the total electric field, $E(t,k)$, is separable into a portion, $E_<(t,k)$, generated by the activity of the source charge density, $\rho(t,k)$, before the observation interval, and a portion, $E_>(t,k)$, generated by the activity

of $\rho(t,k)$ for $t>T_A$. The equations for $E_<$ and $E_>$ are found by substituting the relation

$$E(t,k) = E_<(t,k)+E_>(t,k)$$

into (2-10)

$$ik\,E_<(t,k)+ik\int_{-\infty}^{T_A} dt_1\,E_<(t_1,k)K(t-t_1,k) = 0$$

$$ik\,E_>(t,k)+ik\int_{T_A}^{t} dt_1\,E_>(t_1,k)K(t-t_1,k) = 4\pi\rho(t,k) \quad . \tag{3-32}$$

The contribution of $E_<$ to the total field will be neglected on the grounds that the more significant effect will be due to the more recent activity of ρ during the finite observation interval.

The discrete Fourier transform is defined by the equations

$$E_>(t,k) = \sum_{n=-\infty}^{\infty} E_{>n}(k)e^{-i\omega_n t} \quad , \; T_A\le t\le T_A+T$$

$$E_{>n}(k) = \int_{T_A}^{T_A+T} \frac{dt}{T} E_>(t,k)e^{-i\omega_n t}$$

where $\omega_n = 2\pi n/T$. The discrete Fourier transform of (3-32) entails taking the transform of a convolution integral, which is evaluated in Appendix A. With the use of equation (A-4), the transform of (3-32) is

$$E_{>n}\left[1+T\,K_n-(\tau\,K)_n\right] - \sum_{m\neq n} \frac{E_{>m}}{i\,\omega_{n-m}}\left[K_n-K_m\right] = \frac{-i4\,\pi\,k}{k^2+\alpha^2}\rho_{>n} \tag{3-33}$$

where

$$K_n(k) = \int_0^T \frac{d\tau}{T} e^{i\omega_n\tau} K(\tau,k)$$

$$(\tau\,K)_n(k) = \int_0^T \frac{d\tau}{T} e^{i\omega_n\tau}\,\tau\,K(\tau,k)$$

$$\rho_{>n}(k) = \int_{T_A}^{T_A+T} \frac{dt}{T} \rho(t,k) e^{i\omega_n t} \quad .$$

Equation (3-33) represents a linear matrix equation for the coefficients $\{E_{>n}\}$. To show how to solve such an equation in practice, the analogous equation will be derived for the induced portion of the Green's function. The discrete Fourier transform of $h(\tau,k)$ is

$$h_n(k) = \int_0^T \frac{d\tau}{T} e^{i\omega_n \tau} h(\tau,k) \quad .$$

Combining (1-5) and (3-1), the relationship between $E_{>n}(t,k)$ and $h_n(\tau,k)$ is:

$$E_{>n}(t,k) = \frac{-i4\pi k}{k^2+\alpha^2} \left[\rho(t,k) + \int_{T_A}^{T_A+T} dt_1 h(t-t_1,k) \rho(t_1,k) \right] \quad . \tag{3-34}$$

The discrete transform of (3-34), making use of (A-4), is

$$E_{>n} = \frac{-i4\pi k}{k^2+\alpha^2} \left[\rho_{>n} \left[1+T h_n - (\tau h)_n \right] - \sum_{m \neq n} \frac{\rho_{>m}}{i\omega_{n-m}} \left[h_n - h_m \right] \right] \quad .$$

Again appealing to (A-4), the equation for $\{h_n(k)\}$ from (3-3) is

$$h_n \left[1+T K_n - (\tau K)_n \right] - \sum_{m \neq n} \frac{h_m}{i\omega_{n-m}} \left[K_n - K_m \right] = -K_n(k) \quad . \tag{3-35}$$

To solve (3-35), numerical techniques are employed for computing $\{K_i\}$ and $\{(\tau K)_i\}$, and solving for $\{h_i\}$ $(-i_M \leq i \leq i_M)$. This means approximating $h(\tau,k)$ by a finite number of coefficients, which will be a good approximation provided i_M is chosen so that ω_{i_M} is at least a few plasma frequencies, ω_o.

Figure 3-3 presents $|h_n(k)/\omega_o|^2$ for $k^2\lambda_D^2 = 0.001$ and $T_i = T_e$. Associated with this spectrum is the value $k^2 v_e^2 T^2/2 \simeq 12$ indicating the Green's function has progressed beyond the short-time behavior (the value $T = 50\pi/\omega_o$ is used). It is expected that the first correction $\partial_\tau \mu_1$ should account for much of the frequency broadening in Figure

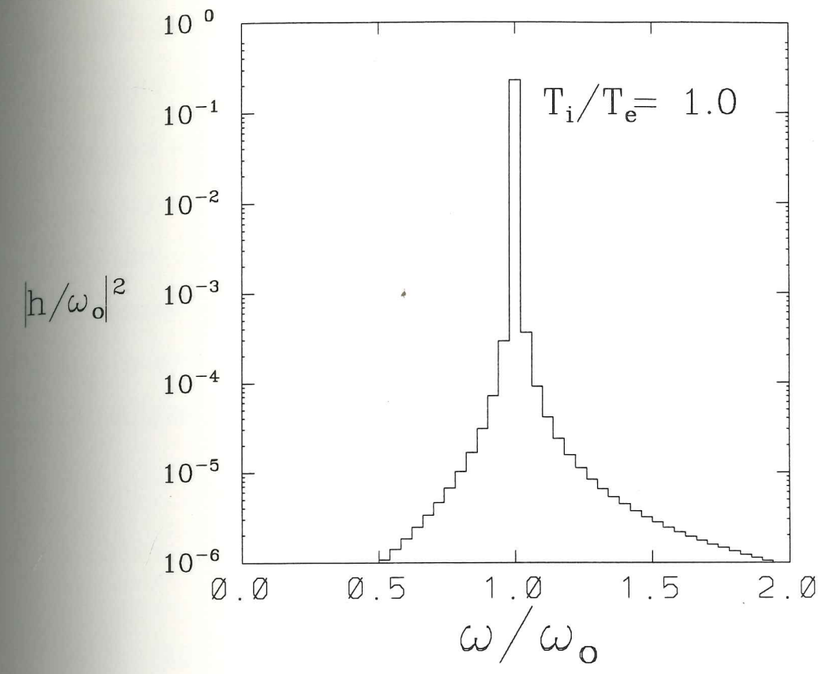

Figure 3-3 $|h_n(k)/\omega_o|^2$ versus ω_n/ω_o for $k^2\lambda_D^2 = 0.001$.

3-3. The solution to (3-24) for n=1, and $v_i=0$ is

$$\partial_\tau \mu_1(\tau,k) = \frac{3}{2}\frac{k^2 v_e^2}{\omega_o}\left[\sin\omega_o\tau - \omega_o\tau\cos\omega_o\tau\right] \quad .$$

The term $\tau\cos\omega_o\tau$ is responsible for the thermal broadening of the frequency peak.

Figure 3-4 considers larger values of $k^2\lambda_D^2$. It is evident that the discrete frequency spectrum provides a more sensitive measure of the Green's function than does Figure 3-1. For example, the appearance of the off-peak frequencies in Figure 3-4a is difficult to observe in Figure 3-1a.

Increased values of wave number result in situations where the asymptotic limit is more quickly attained. This leads to a reduction in the ω_o amplitude and an overall

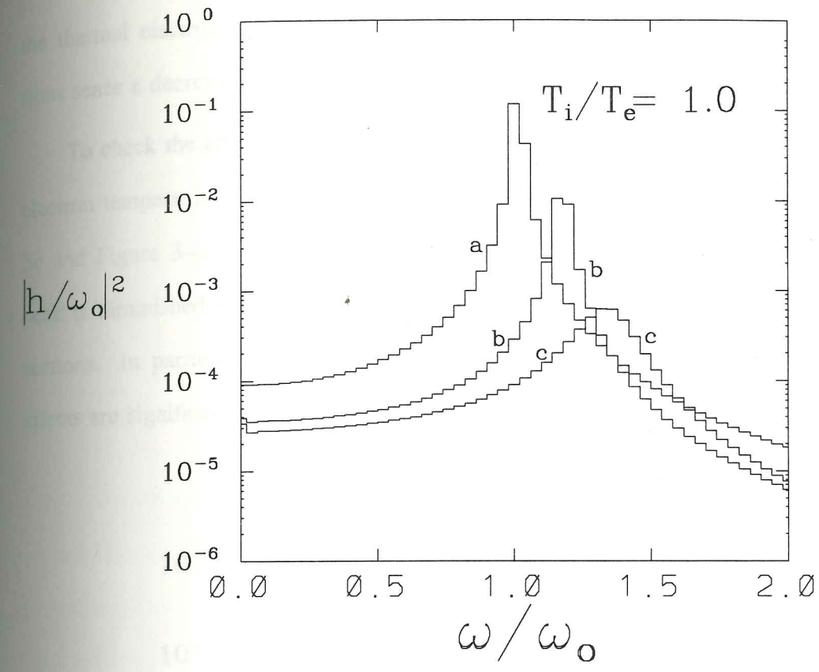

Figure 3-4 $|h_n(k)/\omega_o|^2$ versus ω_n/ω_o (a)$k^2\lambda_D^2 = 0.01$ (b)$k^2\lambda_D^2 = 0.1$ (c)$k^2\lambda_D^2 = 0.2$.

broad frequency spectrum, as seen in Figure 3-4. Furthermore, the ion-acoustic amplitude which contributes to the lowest frequency range (0 to ω_1) increases with k. This can be explained using the simple picture developed in the previous section. For small $k^2v_i^2T^2/2$, the ions approximately remain on the same sheet, and a component of the ion sheet's motion will oscillate at the low frequency of the ion-acoustic mode. The electrons, on the other hand, are highly thermalized and damp the electric field. The damping of the ion-acoustic mode can be diminished by reducing the wavelength of the oscillation (increasing k). This diminishes the effectiveness of the highly thermalized electrons because the low frequency, short wavelength induced electric field appears to these high speed electrons as oscillating rapidly. Hence, on the average,

the thermal electrons contribute less for decreased wavelengths because these electrons sense a decreased mean field.

To check the effects of an increase in ion temperature, Figure 3-5 uses an ion to electron temperature ratio of 10. There is a noticeable difference between Figure 3-5c and Figure 3-4c ($k^2\lambda_D^2=0.2$) in the lowest frequency range where the ion-acoustic peak is diminished in Figure 3-5c. This agrees with the conclusions of the previous sections. In particular, for the study of the asymptotic time limit, the ion thermal effects are significant for $k^2v_i^2T^2/2 \gg 1$, which is the case in Figure 3-5c.

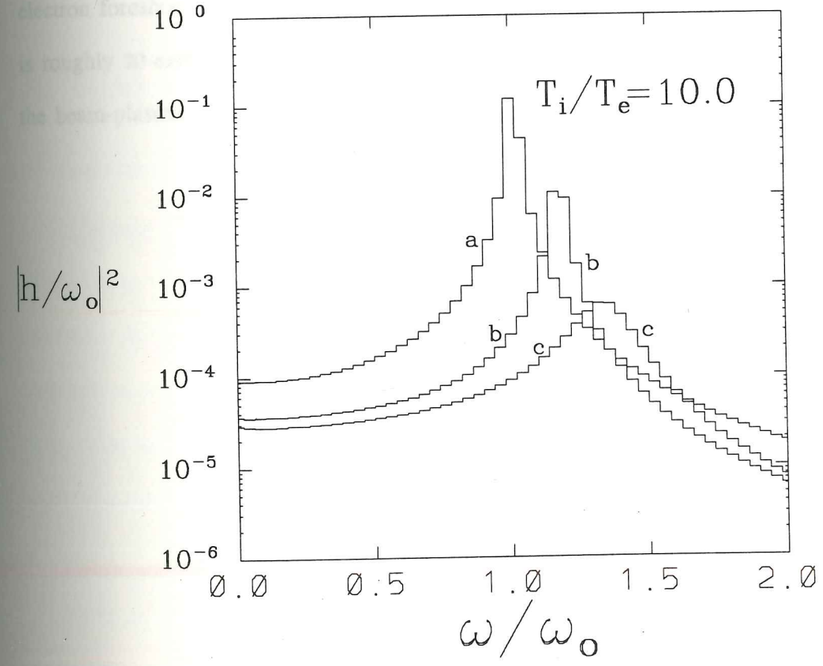

Figure 3-5 $|h_n(k)/\omega_o|^2$ versus ω_n/ω_o (a)$k^2\lambda_D^2 = 0.01$ (b)$k^2\lambda_D^2 = 0.1$ (c)$k^2\lambda_D^2 = 0.2$.

FOUR

Application to the Earth's Electron Foreshock Region

A region where the source problem will be applied is deep within the Earth's electron foreshock shown in Figure 4-1, where the distance Diff defined in the figure is roughly 20 earth radii. To account for the observed electric waves in this region, the beam-plasma theory of *Fuselier et al.* [1985] assumes an electron particle distri-

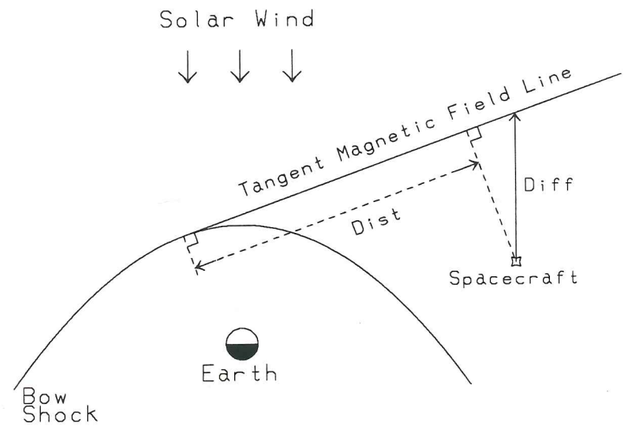

Figure 4-1 Electron foreshock region.

bution which makes the electric field unstable to small perturbations and hence grow in amplitude. However, the unstable distribution used by *Fuselier et al.* [1985] is not supported by the particle observations.

Section 4-3 will apply the theory developed in this thesis to account for the electric wave observations in the foreshock region. First, the observations and the instability calculation of *Fuselier et al.* [1985] will be summarized in Section 4-1. Section 4-2 follows with a summary of the previous chapters needed for the present application. Finally, Section 4-4 compares the source theory to the beam-plasma theory for the case where a low density beam is present. This is relevant near the edge of the electron foreshock region (diff$\leq$5 earth radii).

4-1. Earth's Electron Foreshock Region

a. Summary of Observations

Electrons directed upstream, coming from the earth's bow shock have been observed in the electron foreshock region (see for example *Filbert and Kellogg* [1979]). These electrons may originate from a small fraction of solar wind electrons that reflect when encountering the earth's bow shock and move upstream along the solar wind magnetic field lines to form the electron foreshock. The following summary of observations in the electron foreshock is taken from *Fuselier et al.* [1985].

1. The entire range of frequencies for the plasma oscillations (electrostatic wave activity) measured in the electron foreshock region is from less than $0.1 f_e$ to slightly above the plasma frequency ($f_e = \omega_e/2\pi$). Within this range, there is, predominately, either a high frequency component ($\sim f_e$) or a low frequency

component (~ 15 kHz). The plasma frequency, f_e, in the electron foreshock region is typically 25 to 30 kHz.

2. The bandwidth of the oscillations can be as much as 4 kHz for the low frequency activity (~ 15 kHz) and a few hundred Hz for the high frequency activity (~f_e).

3. The wavelengths are on the order of a few Debye lengths λ_D for the low frequency activity and much greater than λ_D for the high frequency activity. λ_D is typically 10 m in the electron foreshock region.

4. Low frequency plasma oscillations are observed deep (~20 earth radii) in the electron foreshock region, far downstream of the foreshock boundary.

5. The plasma oscillations shift from the high to the low frequency activity. Correlated with this frequency shift is an increase in the flux of energetic electrons streaming from the bow shock. The minimum energy of the electrons streaming from the bow shock decreases as the frequency shifts downward.

b. Beam-Plasma Theory of Fuselier et al.

To account for the observations, *Fuselier et al.* [1985] used the following zeroth-order electron distribution $F_o(v)$ from which the dielectric function was calculated:

$$F_o(v) = F_e(v) + \frac{n_b}{\pi} \frac{C_b}{(v-V_b)^2+C_b^2} \quad . \tag{4-1}$$

$F_e(v)$ is a Maxwellian distribution used to describe the solar wind electron distribution. The second term describes the upstreaming electron distribution (electrons coming from the bow shock) as a Lorentzian beam with n_b, C_b, and V_b as the beam density, thermal speed and beam velocity, respectively. This choice was motivated, in part,

from the guiding center theory which requires that the upstreaming electrons have energies above some cutoff energy in order to reach a particular observation point [*Filbert and Kellogg,* 1979]. V_b is identified as the cutoff velocity. *Fuselier et al.* [1985] solve for the complex frequency roots of the dielectric function and show that a growing mode can exist for reasonable values of n_b, V_b and C_b. The features of this mode are shown to be consistent with the electric wave observations for the entire electron foreshock region (from near the foreshock boundary to deep in the foreshock region). For instance, for $|V_b|/v_e \geq 2$, (v_e is the thermal speed of the solar wind electrons) the oscillation frequency is close to the plasma frequency f_e and the wavelength for maximum growth is much larger than λ_D. As $|V_b|$ is made smaller, the oscillation frequency decreases to below f_e and the wavelength for maximum growth decreases to a few λ_D.

Fuselier et al. [1985] apply the results of the instability calculation to explain the wave activity in the following manner. The particle observations (observation point 5) along with the fact that the low frequencies are observed deep in the electron foreshock region (observation point 4) determine that the minimum energy of the upstreaming electrons decreases as the observation point progresses deeper into the foreshock. This means $|V_b|$ decreases as Diff increases, since V_b is being identified as the cutoff velocity. (Note that there is also an increase in the density of the upstreaming electrons, but only V_b needs to be considered for this discussion). With an increase in Diff, the results of the instability indicate that for the corresponding decrease in $|V_b|$ the wave frequency and wavelength decrease (provided $|V_b| \leq 2v_e$), which accounts for observation points 3-5.

The observed bandwidths (observation point 2) are explained by saying the beam velocity changes during the observation period so that the oscillation frequency sweeps across the frequency range. Consider two values of beam velocity, V_b and $V_b+\delta V_b$ where δV_b denotes the difference of the two velocities and is identified as the variation in the beam velocity. There is a corresponding pair of frequencies, ω and $\omega+\delta\omega$, determined from the dielectric function. The dispersion relation has the property that for fixed δV_b the variation in frequency $\delta\omega$ is larger for smaller $|V_b|$, which accounts for the low frequency wave activity being broad band.

Fuselier et al. [1985] recognize the main weakness in the beam-plasma theory is the lack of evidence for the existence of electron beams deep in the foreshock region. A beam, if present, would show up in the electron distribution as a peak near the beam velocity. This secondary peak (the primary peak is due to the solar wind electrons) is necessary for there to be an instability [*Ichimaru,* 1973]. The measured electron distributions presented by *Fuselier et al.* [1985] show a peak for an observation made near the foreshock edge (Diff ~6 earth radii) and a plateau for an observation made near the middle of the foreshock region (Diff ~16 earth radii). But deep in the foreshock (Diff ~30 earth radii) neither a peak nor a plateau is present. Instead, the distribution of the electrons there shows a suprathermal tail (Figure 4-2). For the cases where no beam is seen, *Fuselier et al.* [1985] suggest a beam does exist, but the beam is not continuous possibly because the electrons come in bursts. Therefore, the beam would not be detected if the temporal resolution of the particle detector is not high enough to monitor the bursts of electrons. Furthermore, the properties of the beam (V_b, n_b, and C_b in (4-1)) may vary during the observation period and make the peak undetectable. For example, the cases where a plateau is present would

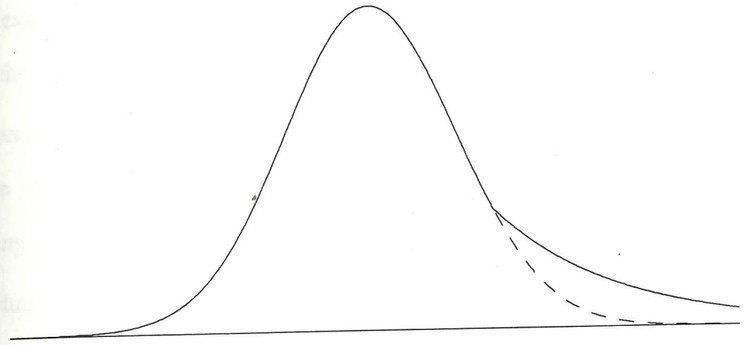

Figure 4-2 Electron distribution deep in electron foreshock region showing a suprathermal tail [*Fuselier et al.*, 1985].

correspond to the beam velocity varying between the velocity limits of the plateau. For observations deep in the foreshock, the beam density and velocity would both have to vary in order to prevent peaks or plateaus from being detected.

The analysis of *Fuselier et al.* [1985] requires a beam to exist deep in the foreshock region. However, this is not substantiated by data. Section 4-3 makes an alternate proposal for producing the waves. This proposal is based on the theory studied in the previous chapters and does not require a beam to be present where the waves are. The analysis assumes that charge fluctuations exist in the upstreaming electron distribution which drive the solar wind plasma, thus resulting in electric wave activity. A possible origin of the assumed fluctuations will be identified in Section 4-4.

4-2. Summary of the Source Problem

The essential points concerning the solution of the source problem were determined in the preceding chapters and are summarized below.

- In general, the Green's function can not be approximated by its asymptotic form for time periods when a source charge density exists (see discussions in Chapter 1 preceding and following equation (1-5)).
- The solution to the source problem has three types of behavior corresponding to the three time limits of the Green's function (see Section 3-1; equations (3-4), (3-7), and (3-9)). These three limits can be present all at the same time because the resultant electric field at time t depends on the source behavior at times before t (see the previous summary point).
- The electric field spectrum will, in general, be non-zero at all frequencies for a thermal plasma, and can be calculated from a matrix relation for the discrete Fourier transform coefficients for a given source charge density (see Section 3-3; equation (3-33)).

Expressions for the Fourier transform coefficients of the electric field were derived in Section 3-3. For completeness, (3-33) is presented here

$$E_{>n}\left[1+T\,K_n-(\tau\,K)_n\right]-\sum_{m\neq n}\frac{E_{>m}}{i\,\omega_{n-m}}\left[K_n-K_m\right]=\frac{-i4\,\pi\,k}{k^2+\alpha^2}\rho_{>n} \qquad (4\text{-}2)$$

where

$$K_n=\int_0^T\frac{d\tau}{T}e^{i\omega_n\tau}K(\tau,k)$$

$$(\tau K)_n = \int_0^T \frac{d\tau}{T} e^{i\omega_n \tau} \tau K(\tau,k)$$

$$\rho_{>n} = \int_{T_A}^{T_A+T} \frac{dt}{T} \rho(t,k) e^{i\omega_n t} \quad .$$

The total field $E_{>n}(k)$ is due to the activity of the source charge density $\rho_{>n}(k)$ for the period $T_A<t<T_A+T$.

$\{E_{>n}\}$ is used for comparison with the measured electric field spectrum. Once $\rho_{>n}$ has been specified, the procedure is to solve (4-2) as a matrix equation for a finite number of terms $\{E_{>n}\}$ (see Section 3-3, where $\{h_n\}$ were calculated in the same fashion). A suitable choice for $\rho_{>n}$ can be based on the observations, as will be shown in Section 4-3.

4-3. Fluctuations in the Upstreaming Electron Distribution

a. Formulation

When formulating the source problem, one must identify the charge density $\rho(t,x)$ of the source. This charge density consists of the electrons traveling upstream from the bow shock showing up in the measured suprathermal tail of the electron distribution. The specification of the x axis is based on the polarization study of *Etcheto and Faucheux* [1984], which shows the electrostatic waves are polarized along the magnetic field. Therefore, the x axis runs parallel to the solar wind magnetic field, and the direction of increasing x is chosen to be from the bow shock into the electron foreshock. Although, the observations are not refined enough to explicitly specify the functional form of $\rho(t,x)$, it was shown by *Etcheto and Faucheux* [1984] that no dependence exists between the upstream wave activity and the distance from the bow

shock measured along the interplanetary magnetic field line which is tangent to the bow shock (Dist defined in Figure 4-1). This observation implies that the proximity of the observation point relative to the bow shock along the magnetic field direction is not a relevant length scale. Consequently, the only length scale that will be considered is a fluctuation length scale (wavelength of fluctuation) in the x direction.

b. Upstreaming Distribution Function

The upstreaming electron distribution is assumed to consist of a constant uniform portion and another which accounts for the spatial and temporal variations of the distribution. The effect of the constant uniform portion on the electric field can be neglected for three reasons. One is that the uniform portion of the solar wind plasma and the upstreaming electron distribution is assumed to be in equilibrium (no net charge density). Therefore, the uniform portion of the plasma will not contribute an electric field. Second, it is assumed here that deep in the electron foreshock region there is no secondary peak in the electron distribution (no beam) and, consequently, the upstreaming electrons do not excite a beam instability. Finally, the number density of the upstreaming electrons deep in the electron foreshock is a small fraction (~ 0.001-0.01) of the solar wind density. Equilibrium of the uniform portion of the plasma means that the fractional difference between the uniform portions of the solar wind ion and electron number densities is also ~ 0.001-0.01. An amount which can be neglected. Hence, only the fluctuating portion of the upstreaming electron distribution will be considered.

Observation points 3 and 4 state that the electric waves deep in the electron foreshock region exist for a narrow range of short wavelengths (on the order of a few

λ_D). This information serves to identify the fluctuation length scale. For the present purpose, the following form of $\rho(t,x)$ is used

$$\rho(t,x) = -e\int dv \cos(k_o x - k_o v(t-T_A)) \hat{f}(v) \quad . \tag{4-3}$$

This charge density is representative of fluctuations in a flow of electrons which vary on a short spatial scale of $2\pi/k_o$ with particle distribution $\hat{f}(v)$. t appears in the form $t-T_A$ because the charge density activity during the observation interval $T_A<t<T_A+T$ is of interest.

An estimate of $\hat{f}(v)$ is based on the uniform portion of upstreaming electron distribution, $f_u(v)$. The average total electron distribution $f_T(v)$ is

$$f_T(v) = F_e(v) + f_u(v) \tag{4-4}$$

where $F_e(v)$ is the Maxwellian distribution associated with the solar wind particles. To approximate the suprathermal tail of $f_T(v)$ illustrated in Figure 4-2, $f_u(v)$ contributes only to the electron distribution at velocities greater than the cutoff velocity v_c ($v_c>0$ for the defined coordinate system), and $f_u(v_c)$ is zero to enforce the condition $f_T(v_c)=F_e(v_c)$ (continuity of the electron distribution). Therefore, $f_u(v)$ is chosen to be

$$f_u(v) = \theta(v-v_c)\frac{n_u}{v_u^2}\left[v-v_c\right]e^{-\frac{v-v_c}{v_u}} \tag{4-5}$$

which enhances the total electron distribution at velocities $v>v_c$ with upstreaming electrons of density n_u and velocity spread v_u.

c. Constraint

A constraint must be placed on the total distribution to ensure there is no peak due to the upstreaming particle enhancement, as required by observations. The constraint requires that $\partial_v f_T$ not vanish for $v>v_c$. The velocity derivative of (4-4) for

velocities $v>v_c$ with (4-5) gives the following restriction on possible plasma parameters for the upstreaming particles

$$\frac{-n}{(2\pi)^{1/2}}\frac{v}{v_e^3}e^{\frac{-v^2}{2v_e^2}}+\frac{n_u}{v_u^2}e^{-\frac{v-v_c}{v_u}}\left[1-\frac{v-v_c}{v_u}\right]\neq 0 \quad . \tag{4-6}$$

Here, n and v_e are, respectively, the particle density and thermal speed of the background solar wind electrons. In general, (4-6) must be satisfied for all velocities greater than the cutoff. This condition is obviously satisfied for $v>v_c+v_u$, since the two terms of (4-6) would then have the same sign. Therefore, for f_u to be considered a possible upstreaming distribution function, its parameters need only be shown to satisfy (4-6) in the velocity range $v_c<v<v_c+v_u$.

Approximating $\hat{f}(v)$ by (4-5), the result of integrating (4-3) is

$$\rho(t,x) = -e\,n_u\left[\beta_1(t-T_A)\cos(k_ox-k_ov_c(t-T_A))+\beta_2(t-T_A)\sin(k_ox-k_ov_c(t-T_A))\right] \tag{4-7a}$$

where

$$\beta_1(t) = \frac{1-k_o^2v_u^2t^2}{(1+k_o^2v_u^2t^2)^2}$$

$$\beta_2(t) = \frac{2k_ov_ut}{(1+k_o^2v_u^2t^2)^2} \quad .$$

The spatial Fourier transform of (4-7a) yields

$$\rho(t,k) = -e\,n_u\pi\,e^{-ikv_c(t-T_A)}\left[\frac{\delta(k-k_o)}{(1+ikv_u(t-T_A))^2}+\frac{\delta(k+k_o)}{(1-ikv_u(t-T_A))^2}\right] \quad . \tag{4-7b}$$

From Section 4-2, equation (4-2) requires $\rho_{>n}(k)$ to calculate $E_{>n}(k)$. Equation (4-2) defines $\rho_{>n}(k)$ as

$$\rho_{>n}(k) = \int_{T_A}^{T_A+T} \frac{dt}{T} e^{i\omega_n t} \rho(t,k)$$

which will be evaluated by numerical integration. The qualitative features of the charge density spectrum is that it is peaked at the frequency $\omega_n = k_o v_c$ with a characteristic width $k_o v_u$. If other functional forms were chosen for the fluctuating portion of the upstreaming electron distribution with qualitatively the same features, the frequency peak and spread for the charge density would still be mainly determined by the characteristic cutoff velocity, thermal speed and fluctuation scale length of the upstreaming distribution. Consequently, (4-7b) has a general significance in regards to the qualitative effect v_c, v_u and k_o has on the electric field spectrum.

d. Results

In the figures to be presented, the plotted electric field amplitudes have been adjusted to correspond to a sine and cosine Fourier series rather than the exponential Fourier series used in the calculations. This permits easy comparison with the reported range of 0.03-0.3 millivolts per meter (mV/m) for the peak electric field amplitudes [*Lacombe et al.*, 1985]. To determine the transformation, one simply compares the two series. The equality

$$E_>(t,x) = E_{c0}(x) + \sum_{n>0} \left(E_{cn}(x) \cos\omega_n t + E_{sn} \sin\omega_n t \right) = \sum_n E_{>n} e^{-i\omega_n t}$$

provides the relationship

$$E_{cn}^2 + E_{sn}^2 = 4 |E_{>n}|^2 \quad , n>0 \quad .$$

It is this quantity which will be graphed.

The solar wind plasma parameters used in this study are: density $n = 10\,cm^{-3}$, thermal speed $v_e = 1200\,km/sec$, and $T_i = T_e$. The x coordinate is permitted to take on any

value of $k_o x = 2\pi m$ (m is any integer), and the starting time of the observation period, T_A, is taken to be an integral multiple of the observation time, T, where $T = 50\pi/\omega_o$ is used. This choice for x and T_A is sufficient for studying the main features of the electric field spectrum. The upstreaming electron velocity parameters v_c and v_u are specified indirectly by taking the characteristic source frequencies, $k_o v_c$ and $k_o v_u$, to be an integral number of the frequency $\omega_1 = 2\pi/T$ (the frequency resolution associated with the observation time T).

i. Effect of Temperature (v_u)

Figure 4-3 considers $k_o\lambda_D \simeq 0.32$ ($k_o^2\lambda_D^2 = 0.1$) using a density for the upstreaming electrons of $n_u = 0.001n$, a cutoff velocity $v_c \simeq 2v_e$ ($k_o v_c = 16\omega_1$), and two values for the thermal speed of the upstreaming distribution, $v_u \simeq 0.13$ and $0.25v_e$ ($k_o v_u = 1$ and $2\omega_1$). The graph with the lower value of v_u clearly displays two dominant frequency peaks corresponding to the characteristic background solar wind response (high frequency peaks present in the Green's function), and a peak associated with the driving frequency (activity below the plasma frequency). Increasing the thermal speed, v_u, affects the spectrum by broadening the low frequency activity and reducing the amplitude due to the wave energy being distributed over a broader frequency range. Based on the reported range of 0.03- 0.3 mV/m for the peak electric field amplitudes [*Lacombe et al.,* 1985], Figure 4-3 provides an estimate for the thermal speed of the upstreaming electrons. The lower value of $v_u = 0.13\,v_e$ used in Figure 4-3 is a good estimate because it gives amplitudes that agree with the reported range of *Lacombe et al.* [1985]. The constraint (4-6) provides a lower limit on allowable values for v_u by considering when (4-6) is not satisfied. From (4-5), the upstreaming distribution will be peaked at v near v_c for small v_u. Hence, an estimate for the lower limit is found by

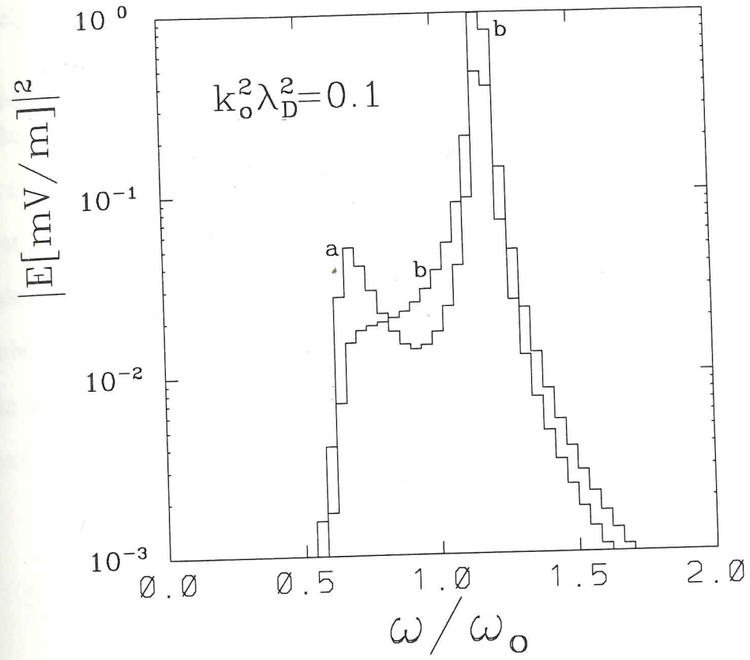

Figure 4-3 Electric field spectrum comparing two values of thermal speed for the upstreaming electron distribution with $k_o^2\lambda_D^2 = 0.1$: (a) $v_u = 0.127\, v_e$ (b) $v_u = 0.253\, v_e$.

expanding (4-6) about $v = v_c$, which gives to lowest order the expression

$$\frac{-n}{(2\pi)^{1/2}} \frac{v_c}{v_e^3} e^{\frac{-v_c^2}{2v_e^2}} + \frac{n_u}{v_u^2} \quad . \tag{4-8}$$

For the constraint not to be satisfied, (4-8) must equal zero, which is then solved for the minimum allowable value for v_u

$$\left[\frac{v_u^2}{v_e^2}\right]_{min} = \frac{1}{(2\pi)^{1/2}} \frac{n_u}{n} \frac{v_e}{v_c} e^{\frac{v_c^2}{2v_e^2}} \quad .$$

For the parameters of Figure 4-3, $(v_u)_{min} \sim 0.04\, v_e$, placing the v_u values used in Figure

4-3 safely above the estimate on the minimum allowable v_u.

ii. Effects of Density and Cutoff Velocity (n_u and v_c)

The three graphs in Figure 4-4 represent spectra from different observation points in the electron foreshock region. The graphs are distinguished by three different values of the cutoff velocity, $v_c \approx 2.0, 1.5, 1.0\, v_e$, with respective values of increasing upstreaming electron density, $n_u = 0.001, 0.003, 0.0035\, n$. These correspond to three observation points each progressively deeper into the foreshock region (larger Diff), in accordance with the particle observations stated in point 5. As the number of lower energy electrons increases, the spectrum peak associated with the driving

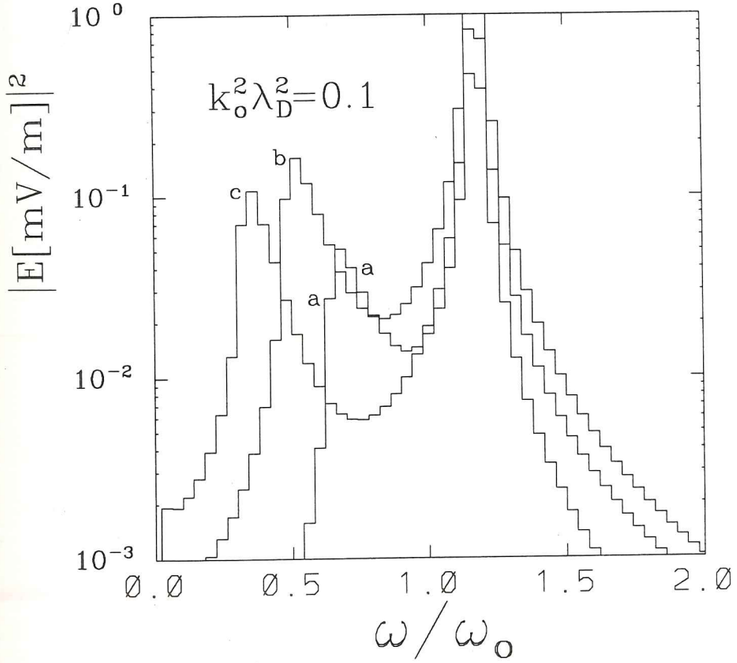

Figure 4-4 Electric field spectrum comparing three sets of plasma parameters for the upstreaming electron distribution with $k_o^2\lambda_D^2 = 0.1$ and $v_u = 0.127 v_e$: (a) $v_c = 2.0\, v_e$, $n_u = 0.001\, n$ (b) $v_c = 1.5\, v_e$, $n_u = 0.003\, n$ (c) $v_c = 1.0\, v_e$, $n_u = 0.0035\, n$.

source charge density shifts in frequency from near (but still below) the plasma frequency to increasingly farther below the plasma frequency while maintaining a significant intensity. Therefore, the present theory does show a shifting of the frequency activity from high to low frequencies (see the wave observations stated in point 5) with maximum amplitudes within the range reported by *Lacombe et al.* [1985]. Finally, Figure 4-5 demonstrates the shift in frequency for a different wave number, $k_o^2\lambda_D^2$=0.2. Here it is noticed that the amplitude of the low frequency peak is actually larger than the high frequency peak, meaning the driving frequency is dominant.

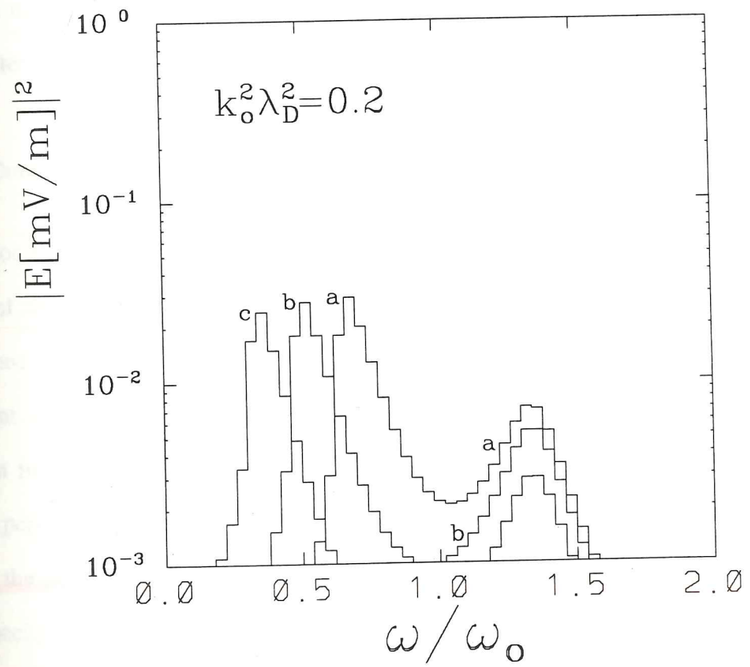

Figure 4-5 Electric field spectrum comparing three sets of plasma parameters for the upstreaming electron distribution with $k_o^2\lambda_D^2 = 0.2$ and $v_u = 0.089\, v_e$: (a) $v_c = 1.4\, v_e$, $n_u = 0.001\, n$ (b) $v_c = 1.1\, v_e$, $n_u = 0.0013\, n$ (c) $v_c = 0.7\, v_e$, $n_u = 0.0015\, n$.

e. Discussion

The results of this section show that including small fluctuations in the upstreaming electron distribution can lead to measurable electric waves without the electrons being organized as a beam. Moreover, the features qualitatively agree with the observed wave activity using source properties inferred from the observations. There remains to be considered two important issues. One is to identify a possible origin of the assumed fluctuations. The other is to apply the source theory for the wave activity observed near the electron foreshock edge (diff $\lesssim 5$ earth radii), where a low density beam is present and is likely to cause an instability. Both of these issues will be discussed in Section 4-4 by comparing the source and beam-plasma theories in greater detail.

4-4. Comparison of Source Theory and Beam-Plasma Theory

For the case where the plasma includes a low density beam (such as near the edge of the electron foreshock), there are seemingly two perspectives on which to base one's analysis. On the one hand, one may consider the beam as part of the ambient (or zeroth-order) plasma, which is the basis for beam-plasma theory. Given that an instability exists, this theory then may account for the wave generation. The other perspective is motivated by the present development of the source problem. Since the beam is a small contribution to the plasma as compared to a large Maxwellian background (such as the ambient solar wind), one may consider the beam as a source of injected charge effective in driving electric wave activity. To relate these two theories, a closer look at their basic limitations and applicability will be taken.

a. Ordering for Beam-Plasma Theory

Under consideration are two linear approximations to the same basic non-linear equations with the exception that the Vlasov equation was extended to be inhomogeneous for the source problem. The approximation made is different in each case, as seen by identifying the zeroth-order quantities. For the beam-plasma theory, both the Maxwellian background and the uniform beam distribution are components of the zeroth-order plasma. In regards to the spatial particle densities which determine the electric field, the approximation means that the first-order density for a given particle species is much smaller than the individual components of the ambient plasma. This sets the scale of the first-order density contribution as much smaller than the zeroth-order beam density. Formally introducing an ordering parameter λ to keep track of the density scale in an expansion, Gauss' law becomes

$$\partial_x E(t,x) = 4\pi \sum_a q_a \int dv\, f_a(t,x,v) = 4\pi \left\{ \lambda \rho^{(1)} + \lambda^2 \rho^{(2)} + \cdots \right\} \tag{4-9}$$

where $\rho^{(m)}$ is the order m contribution to the total charge density. No zeroth-order term appears in (4-9) because the ambient plasma is assumed to be charge neutral. Terms of second-order and higher are neglected in the linear approximation. From this, one can estimate that the minimum amplitude electric field to which the theory is sensitive (the degree of accuracy of the theory) is of order λ^2, since this is the lowest order charge density that is neglected. This estimate really only has meaning while the non-linear terms ($m>1$) are negligible. Under the assumption that the zeroth-order plasma is responsible for an instability, the non-linear terms will eventually be significant, marking the breakdown of this linear theory.

b. Ordering for Source Theory

The linear approximation made for the source theory differs from the beam-plasma theory in that the zeroth-order plasma consists of just the Maxwellian background. Densities on the scale of the beam are taken to be of first order, with a corresponding ordering parameter, $\hat{\lambda}$. Comparison to beam-plasma theory shows that the charge density term of order $\hat{\lambda}$ (from source theory) is much larger than the term of order λ appearing in (4-9). The sensitivity of source theory is estimated to be of order $\hat{\lambda}^2$, directly analogous to beam-plasma theory. The distinction between the two theories is now clear. Beam-plasma theory is capable of describing wave activity in the amplitude range from orders λ^2 to λ, whereas the source theory applies to activity from orders $\hat{\lambda}^2$ to $\hat{\lambda}$. Therefore, the two theories are compatible in that they describe different intensity levels in the plasma. The source theory describes a higher intensity level than the beam-plasma theory because the density of order $\hat{\lambda}$ is greater than the density of order λ. To estimate the two intensity levels, consider the density ranges for the two orderings using a beam density of $10^{-3}\,n$ (n is density of Maxwellian background). With this beam density, the approximate density range for which the source problem applies is 10^{-6}-$10^{-3}\,n$. Gauss' law provides the corresponding electric field intensity range of 10^{-6}-$10^{-3}(2\,e\,n\,L)$, where L is a characteristic wavelength. For example, using a characteristic wavelength of $L = 500\,m$ and $n = 10\,cm^{-3}$, the range of electric field intensity is 0.015-15 mV/m. This gives an estimate that defines the higher intensity range. The lower intensity range is estimated by recalling that the density of order λ of the beam-plasma theory is much less than the beam density. If the density of order λ is, say, a factor of 10^{-2} times the beam density, the lower intensity range is 1.5×10^{-3}-1.5×10^{-1} mV/m.

Although the two theories do not directly trace the wave activity as it might develop from low to high intensities, it is expected that the transition does occur based on the above estimate for the intensity levels of the two theories. Electric field amplitudes in the electron foreshock region near the foreshock boundary, where a beam is present, are typically a few millivolts per meter [*Etcheto and Faucheux,* 1984], which places the measurement in the high intensity level (described by source theory). This motivates the picture that the wave activity originates at the low intensity level by means of an instability as given by beam-plasma theory. While the activity is described by beam-plasma theory, it lies below the threshold intensity at which the source problem is applicable. The wave activity then increases into the high intensity level, the domain of the source theory. Therefore, the source theory can be used to compute the field spectrum with the source charge density being generated by the wave activity that arises from the beam-plasma instability. Here, the source theory is used to describe the final stable state of the wave activity. Chapters 1 and 2 discussed many uses of the source term for the source problem. There it is stated that the source term can be due to particles injected into the ambient particles, or it can represent a variety of physical processes that has the effect of driving the plasma. The present application belongs to the latter category and describes the introduction of particle distribution effects from terms neglected in the linear approximation. This statement is more clearly understood in what follows.

Consider the ordering of the distribution function. Of interest is the situation where the uniform portion of the beam distribution is already present and established, which means the uniform portion of the beam is not part of the particle source term ζ_a. This is in contrast to a study of the initial injection of a beam, which monitors the

equilibration of the uniform plasma components. Therefore, the ordering of the distribution function is:

$$f_a(t,x,v) = F_a^{(0)}(v) + \hat{\lambda} F_a^{(1)}(v) + \hat{\lambda} f_{B,a}^{(1)}(v) + \sum_{m=1}^{\infty} \hat{\lambda}^m f_a^{(m)}(t,x,v) \quad . \tag{4-10}$$

Notice the first three terms of (4-10) are spatially uniform plasma components. $F_a^{(0)}+\hat{\lambda} F_a^{(1)}$ is the uniform distribution of the solar wind plasma for the case of the electron foreshock region. $\hat{\lambda} f_{B,a}^{(1)}$ is the uniform beam distribution for species a, which for the source problem is a first-order quantity. The first-order term for the solar wind plasma, $\hat{\lambda} F_a^{(1)}$, is necessary so that the uniform portion of the plasma can be in equilibrium. Equilibrium is arranged by assuming the uniform portion of the plasma is charge neutral.

Substituting (4-10) into Gauss' law then gives

$$\partial_x E(t,x) = 4\pi \sum_a \sum_{m=1}^{\infty} q_a \int dv \hat{\lambda}^m f_a^{(m)}(t,x,v) \tag{4-11}$$

indicating the electric field expansion has the form

$$E(t,x) = \sum_{m=1}^{\infty} \hat{\lambda}^m E^{(m)}(t,x) \quad . \tag{4-12}$$

The inhomogeneous Vlasov equation with (4-10) and (4-12) becomes

$$(\partial_t + v\partial_x)\hat{\lambda} f_a^{(1)} + \hat{\lambda} \frac{q_a}{m_a} E^{(1)} \partial_v F_a^{(0)} = \tilde{\zeta}_a \tag{4-13}$$

where symbolically

$$\tilde{\zeta}_a = \hat{\lambda} \zeta_a^{(1)} + \text{Higher Order} \quad . \tag{4-14}$$

It is useful to distinguish between two types of terms in (4-14). First, there are the terms coming from the $\hat{\lambda}$ expansion of the particle source term ζ_a. Since the uniform portion of the beam is treated as already present in the system, ζ_a pertains only to the

injection of a fluctuating portion of a particle distribution. The other terms in (4-14) are the higher order terms arising from the functions $f_a^{(m)}$ and $E^{(m)}$. Both types of terms contribute to higher order in (4-14), and would normally be neglected altogether in the linear approximation. But in light of the instability that exists at the low intensity level, the possibility that the cumulative effect of the higher order terms results in a contribution of order $\hat{\lambda}$ is proposed. This statement represents a gross simplification of the non-linear effects that describe the wave activity as it progresses from the low intensity instability level to a stable plasma configuration. Nonetheless, such a premise will serve to link the two linear theories, with the source theory describing the stable plasma configuration from which the wave spectrum is calculated.

To pursue this analysis the first-order term $\zeta_a^{(1)}$ is taken to be zero. This restricts the study to waves which originate solely from the higher order effects. Therefore, the basic first-order relations from (4-11) and (4-13) are precisely the same equations studied in Chapters 1-3 with $\tilde{\zeta}_a$ as the source term. However, the complication exists that $\tilde{\zeta}_a(t,x,v)$ is not known. Even though it is in principle calculable in terms of an expansion, there is no guarantee that such a route would prove fruitful. The aim of this section is not to determine $\tilde{\zeta}_a$, but to establish one simple and informative fact. This fact has to do with the ability to solve for a portion of the particle distribution function. The inversion of (4-13) for $f_a^{(1)}(t,k,v)$ is given by (2-9). In particular, the following term appears

$$\int_{-\infty}^{t} dt_1 \, e^{-ikv(t-t_1)} \tilde{\zeta}_a(t_1, k, v) \tag{4-15}$$

which is the part of the particle distribution function due to the source term and determines the source charge density, $\rho(t,x)$. Consider the activity of $\tilde{\zeta}_a$ before the observation time $t=T_A$. Then for $t \geq T_A$, its contribution to (4-15) is

$$\int_{-\infty}^{T_A} dt_1 \, e^{-ikv(t-t_1)} \tilde{\zeta}_a(t_1, k, v) \tag{4-16}$$

which satisfies the free-streaming Vlasov equation given by (1-4).

$$(\partial_t + ikv) \int_{-\infty}^{T_A} dt_1 \, e^{-ikv(t-t_1)} \tilde{\zeta}_a(t_1, k, v) = 0 \quad . \tag{4-17}$$

Equation (4-17) is the same equation satisfied by the fluctuating portion of the upstreaming electron distribution used in Section 4-3 for the region deep in the electron foreshock (the distribution function appears in the integrand of (4-3)). In fact, a further point is that the same qualitative form assumed in (4-3) is expected to apply in this case of a low density beam causing an instability. For one thing, the instability has the largest growth rates for some characteristic wave number. It is this wave number that gets identified as k_o in (4-3). With a given k_o for which the beam-plasma theory is unstable, a wave with predominantly one phase velocity results [*Ichimaru,* 1973]. In regards to (4-3), this means that $\hat{f}(v)$ serves to specify the velocity distribution corresponding to the phase velocity distribution.

It should be emphasized that the non-linear effects, which here are being ignored, may change the details of these statements. Consequently, these results apply only if the main features of the instabilities here discussed are preserved as the wave activity progresses into the high intensity level. Further note that the frequencies

given by the beam-plasma theory do not directly influence the portion of the wave activity due to (4-16). This is because (4-16) only includes the activity of $\tilde{\zeta}_a$ before $t=T_A$ and evolves according to (4-17) during the observation period $T_A<t<T_A+T$. Only the spatial and phase velocity properties of the instability directly affect this portion of the wave activity.

An overall description of the wave activity in the electron foreshock region is arrived at from the relationship between source theory and beam-plasma theory, and the similarity between (4-16) and the fluctuating distribution used in the region deep in the electron foreshock region appearing in the integrand of (4-3). Recall that the region for which no beam is observed (deep in the electron foreshock region) the wave activity was shown in Section 4-3 to be well described by including a fluctuating distribution with its assigned properties. An explanation for this driving distribution follows from assuming that a beam exists nearer to the bow shock (smaller Dist in Figure 4-1) than the observation point. Then, at the location of the beam, the application of beam-plasma theory determines if an instability is at work. Assuming an instability exists, the instability initiates the fluctuations in the distribution function that drive the source theory. The explanation for why a beam is not present deep in the foreshock region is that the higher order terms in (4-14) include the effect the waves have on dispersing (spreading or smearing out) the velocity distribution of the electrons. Therefore, the peak in the electron distribution assumed to exist at small Dist (defined in Figure 4-1) disperses to a suprathermal distribution (Figure 4-2) with a fluctuating portion as each parcel of upstreaming electrons progresses into the electron foreshock region.

This reasoning helps to understand the parameters used in Section 4-3. Again, k_o is related to a wave number that corresponds to the maximum growth rates calculated from the beam-plasma theory [*Fuselier et al.*, 1985]. As for the thermal speed v_u, a result of the computations in Section 4-3 was that v_u of about $0.1\,v_e$ is needed to account for the observed level of wave activity. Recalling that $\hat{f}$ is a measure of the phase velocity distribution of the driver, this v_u is consistent with there being only a small range of phase velocities that are unstable in the beam-plasma theory. Finally, the constraint placed on the parameters to ensure no beam was present represents the effect the higher order terms have on dispersing the beam, which results in the suprathermal tail.

For the region where a beam is present (near the edge of the electron foreshock region), the source theory indicates there are two effects of the driving term $\tilde{\zeta}_e$. One is analogous to the behavior derived for the region deep in the foreshock, which is due to the driving fluctuation in (4-16). Based on the results of Section 4-3, the peak in the wave activity due to this portion of the driver occurs at the frequency $\omega_{peak} \simeq k_o v_c$. Roughly, v_c is close to the peak of the phase velocity distribution $\hat{f}$ for small v_u. This means that $\hat{f}$ peaks at a phase velocity approximately equal to ω_{peak}/k_o. Recall that, this peak in $\hat{f}$ corresponds to the phase velocity of the wave with the largest growth rate from beam-plasma theory. Therefore, ω_{peak} is approximately equal to the oscillation frequency determined from beam-plasma theory because the phase velocity is the angular frequency divided by the wave number. Relating this to an earlier comment, it is noted that even though the frequency given by beam-plasma theory does not directly influence the wave activity due to (4-16), the corresponding

frequency spectrum calculated from the source theory has a peak at approximately the beam-plasma frequency. As for the effect of the activity of the source term during the observation time $T_A<t<T_A+T$, this may directly depend on the frequency given by beam-plasma theory. Therefore, this latter activity may also drive the plasma at approximately the same peak frequency as does (4-16).

In summary, the point that the beam-plasma frequency is approximately the frequency for which the source theory has a spectrum peak means the strong points of beam-plasma theory to account for the measured frequency peak applies here to this overall description of the electron foreshock. The shortcoming of the beam-plasma theory, that it is not able to explain wave activity where no beam is observed, is resolved by assuming that the beam which causes the instability does not penetrate the electron foreshock because it disperses in velocity to a suprathermal tail with a fluctuating portion. It is this fluctuating portion with its characteristic wavelength that drives the wave activity as calculated by source theory, and marks an important difference from the beam-plasma theory which assumes the upstreaming electron distribution is spatially uniform.

As for the activity near the foreshock boundary, the velocity dispersion of the beam is expected to be less effective here because its large beam speed is in a velocity range where few solar wind electrons contribute to the distribution. Therefore, the dispersion process is expected to take a longer time to blend the beam into the solar wind distribution in order to eliminate the electron distribution peak. This explains why a beam can exist in the edge of the electron foreshock but not deep in the foreshock region. Some details can not be determined from this combined

theory. These mainly have to do with the specifics of the velocity dispersion of the beam. This matter is a prime candidate for future study.

FIVE

Conclusion

This thesis defined and formulated the source problem in a precise manner. Comparisons were made to the Landau problem, showing in Chapter 1 that the Landau problem is obtainable using the formalism of the source problem with the appropriate source charge density. Chapters 1 and 2 introduced the Green's function emphasizing its relationship to the dielectric function of the Landau problem. In particular, the limitation of simply considering the roots of the dielectric function is that the effects of a source charge density would not be properly described for periods when the source charge density is non-zero. Chapter 3 confirmed this by studying the Green's function in three temporal limits: short, intermediate and asymptotic, which showed that the characteristic frequency of the Green's function changes in time.

The result that there are characteristic time scales which distinguish the frequencies of the different time intervals may have important consequences to plasmas other than the equilibrium plasma considered in this thesis. It was shown that thermal effects were less significant in the short-time and intermediate time behavior than for the asymptotic time behavior. Consider applying this to, for example, a plasma that

has an ion component that drifts relative to the other plasma components so as to cause an instability. The growth rate should be greater for the short-time and intermediate time behavior because the thermal effects of the plasma components have not fully developed to the level that exists in the asymptotic limit. Taking the example one step further, if the temperatures of the plasma components were such that an instability were prohibited in the asymptotic limit, it still is possible for an instability to exist in the other time limits because thermal effects are less significant.

Chapter 3 derived relations to calculate electric field spectra. These relations were applied to the region deep in the Earth's electron foreshock in Chapter 4 to find spectra that generally agreed with the reported observations. The major contribution was the suggestion that wave activity can be caused by fluctuations that drive the plasma. This explains how waves can exist in regions where no apparent instability is present.

This thesis restricted itself to the case of electrostatic waves in an unmagnetized plasma. A natural extension of the source problem for future work would be to include an ambient magnetic field and to study electromagnetic as well as electrostatic waves.

References

Abramowitz, M. and I. A. Stegun, eds., *Handbook of Mathematical Functions,* U. S. National Bureau of Standards, 1964, Dover, New York, 1965.

Cambou, F., V. S. Dokoukine, J. Lavergnet, R. Pellat, H. Reme, A. Saint-Marc, R. Z. Sagdeev and I. A. Zhulin, ''General description of the Araks experiment,'' *Ann. Géophys.* **36 no. 3**, 271, 1980.

Dahlquist, G. and Å. Björck, transl. by N. Anderson, *Numerical Methods,* Prentice-Hall, Englewood Cliffs, 1974.

Etcheto, J. and M. Faucheaux, ''Detailed study of electron plasma waves upstream of the Earth's bow shock,''

Filbert, P. C. and P. J. Kellogg ''Electrostatic noise at the plasma frequency beyond the Earth's bow shock,'' *J. Geophys. Res.* **84**, 1369, 1979.

Fried, B. D. and G. J. Culler, ''Plasma oscillations in an external electric field,'' *Phys. Fluids* **6**, 1128, 1963.

Fuselier, S. A., D. A. Gurnett and R. J. Fitzenreiter, ''The downshift of electron plasma oscillations in the electron foreshock region,'' *J. Geophys. Res.* **90**, 3935, 1985.

Harvey, C. C., J. Etcheto, Y. de Javel, R. Manning and M. Petit, ''The ISEE electron density experiment,'' *IEEE Trans. Geos. Elect.* **GE-16 no. 3**, 231, 1978.

Ichimaru, S., *Basic Principles of Plasma Physics: A Statistical Approach,* Benjamin/Cummings, London, 1973.

Klimas, A. J., ''The electron foreshock,'' *Collisionless Shocks in the Heliosphere: Reviews of Current Research, Geophys. Monogr. Ser.,* vol. 32, edited by B. T. Tsurutani and R. G. Stone, p.237, AGU, Washington D.C., 1985.

Krall, N. A. and A. W. Trivelpiece, *Principles of Plasma Physics,* McGraw-Hill, New York, 1975.

Lacombe, C., A. Mangeney, C. C. Harvey and J. D. Scudder, ''Electron plasma waves upstream of the Earth's bow shock'' *J. Geophys. Res.* **90**, 73, 1985.

Landau, L. D., "On the vibrations of the electronic plasma," *J. Phys. (U.S.S.R.)* **10**, 25, 1946.

Morse, P. M. and H. Feshbach, *Methods of Theoretical Physics,* pt. I, McGraw-Hill, New York, 1953.

Neubert T., W. W. L. Taylor, L. R. O. Storey, N. Kawashima, W. T. Roberts, D. L. Reasoner, P. M. Banks, D. A. Gurnett, R. L. Williams and J. L. Burch, "Waves generated during electron beam emissions from the space shuttle," *J. Geophys. Res.* **91**, 11,321, 1986.

Nicholson, D. R., *Introduction to Plasma Theory,* John Wiley & Sons, New York, 1983.

Weitzner, H., "Green's function for the linearized Vlasov equation," *Phys. Fluids* **5**, 933, 1962.

Weitzner, H., "Long-wavelength plasma oscillations," *Phys. Fluids* **7**, 476, 1964.

APPENDIX **A**

Discrete Transform of Convolution Integral

In this appendix the discrete Fourier transformation of a convolution integral needed in Chapter 3 is evaluated. For an arbitrary pair of functions of time, say $\alpha(t)$ and $\beta(t)$, the following operation defines the transform of the desired convolution integral

$$(\alpha,\beta)_n \equiv \int_0^T \frac{dt}{T} e^{i\omega_n t} \int_0^t dt_1 \alpha(t)\beta(t-t_1) \qquad \text{(A-1)}$$

with T and ω_n defined in Chapter 3. Owing to the symmetry of the convolution integral:

$$\int_0^t dt_1 \alpha(t_1)\beta(t-t_1) = \int_0^t dt_1 \beta(t_1)\alpha(t-t_1) \quad ,$$

it is noted that (A-1) is symmetric with respect to interchanging α and β

$$(\alpha,\beta)_n = (\beta,\alpha)_n \quad . \qquad \text{(A-2)}$$

A delta function can be inserted into (A-1) to give

$$(\alpha,\beta)_n = \int_0^T \frac{dt}{T} e^{i\omega_n t} \int_0^t dt_1 \int_0^T dt_2 \alpha(t_1)\beta(t_2)\,\delta(t-t_1-t_2)$$

$$= \sum_{j=-\infty}^{\infty} \beta_{j+n} \int_0^T \frac{dt_1}{T} e^{i\omega_{j+n}t_1} \alpha(t_1) \int_{t_1}^T dt e^{-i\omega_j t} \qquad \text{(A-3)}$$

where the latter equality is gotten by substituting the discrete transform representation of the delta function

$$\delta(t-t_1-t_2) = \frac{1}{T} \sum_{j=-\infty}^{\infty} e^{-i\omega_j(t-t_1-t_2)}$$

and by interchanging the summation and integration operations. Performing the t integration, the form of (A-3) used in Chapter 3 is:

$$(\alpha,\beta)_n = T\alpha_n\beta_n - \beta_n \int_0^T \frac{dt_1}{T} e^{i\omega_n t_1} t_1 \alpha(t_1) + \sum_{j\neq 0} \left[\frac{\alpha_n\beta_{j+n} - \alpha_{j+n}\beta_{j+n}}{i\omega_j} \right] . \qquad \text{(A-4)}$$

Equation (A-4) does not manifest the symmetry stated in (A-2). Another form which readily shows this symmetry is obtained by eliminating the summation in the following expression in favor of an integral

$$\sum_{j\neq 0} \frac{\beta_{j+n}}{i\omega_j} = -\int_0^T \frac{dt}{T} e^{i\omega_n t} \beta(t) \sum_{j\neq 0} \frac{e^{-i\omega_j t}}{i\omega_j} \qquad \text{(A-5)}$$

where the β_{j+n} were substituted in terms of the inverse transform. By noting that the discrete Fourier representation of the variable t is

$$t = \frac{T}{2} + \sum_{j\neq 0} \frac{e^{-i\omega_j t}}{i\omega_j} \quad ,$$

one can write (A-5) as

$$\sum_{j\neq 0} \frac{\beta_{j+n}}{i\omega_j} = \frac{T}{2}\beta_n - \int_0^T \frac{dt}{T} e^{i\omega_n t} t\beta(t) \quad . \qquad \text{(A-6)}$$

Substitution of (A-6) into (A-4) gives an alternate expression for the discrete transform of the convolution integral

$$(\alpha,\beta)_n = \frac{3}{2}T\alpha_n\beta_n - \int_0^T \frac{dt}{T} e^{i\omega_n t} t \left[\alpha_n\beta(t) + \beta_n\alpha(t)\right] - \sum_{j\neq 0} \frac{\alpha_{j+n}\beta_{j+n}}{i\omega_j} \qquad \text{(A-7)}$$

which is manifestly symmetric with respect to interchanging α and β.

Vita

Michael Joseph Pangia was born in Stamford, Connecticut in 1958 to Pauline M. and Michael A. Pangia. He attended public schools in Stamford and graduated from Rippowam High School in 1976. Later that year, he entered college at the Cooper Union, School of Engineering, New York, New York, where he studied Mechanical Engineering. After four years there, he received the Bachelor of Engineering degree. In 1980 he began graduate studies in Physics at Michigan State University, East Lansing, Michigan, and received the Master of Science degree after two years. In 1982 he continued graduate studies in Physics under G. K. Parks at the University of Washington, Seattle, Washington, and received the Doctor of Philosophy degree in 1988.